Optimization of Biogenic Supplementary Cementitious Materials in Concrete prepared from East-Indian Lemon Grass (Cymbopogon flexuosus) and Poultry Litter using Response Surface Methodology

Neelam Bora
Tezpur University
Niran Daimary
Tezpur University
Mondita Athparia
Tezpur University
M. K. Loganathan
KU: Kaziranga University
Rupam Kataki
rupamkataki@gmail.com

Tezpur University https://orcid.org/0000-0003-0114-3858

Research Article

Keywords: Calcined Lemon Grass biochar, Poultry Litter Ash, Supplementary Cementitious Material, Biochar ash, Curing Period, Water-cement ratio

Posted Date: September 11th, 2023

DOI: https://doi.org/10.21203/rs.3.rs-3314588/v1

Version of Record: A version of this preprint was published at Energy, Ecology and Environment on February 20th, 2024. See the published version at https://doi.org/10.1007/s40974-024-00320-0.

Abstract

Developing high-quality construction materials from agricultural waste as a substitute of conventional cement is receiving immense global interest in recent times, due to issues like greenhouse gas emissions and extensive energy consumption during cement production. This study aims to investigate the compressive, flexural and split tensile strengths of concrete through the utilization of bio-based products prepared from East-Indian lemon grass (*Cymbopogon flexuosus*) and poultry litter as supplementary cementitious materials (SCMs). The optimization process involves Central Composite Design (CCD) based Response Surface Methodology (RSM) for modelling and statistical analyses using experimental data from the study. Analysis of variance (ANOVA) revealed the model's significance, with coefficient of determination (R^2) of 0.9956. The individual and synergistic effects of the considered factors on compressive strength were analyzed using three-dimensional response surface plot. Based on RSM analysis, concrete prepared by substituting 17.57% of Ordinary Portland cement with SCM (which was cured for 25.82 days with a water-cement ratio of 0.54), yielded the optimum compressive, flexural and split tensile strengths of 33.94 ± 0.12, 8.78 ± 0.02 and 3.06 ± 0.02 N/mm² respectively. Furthermore, the SCM-mixed concrete exhibited enhanced durability properties of the concrete structure. The findings also demonstrate the robustness of RSM as a significant tool for optimization of concrete performance. Moreover, the characterization results of pyrolytic lemon grass bio-oil (LG-BO) confirms its bioenergy potential thereby suggesting its diverse utilization in various applications.

Article Highlights

- Use of lemon grass shows a potential integrated approach towards production of supplementary cementitious material (SCM) and biofuel.
- Partially substituting cement with SCM derived from lemon grass & poultry litter enhanced mechanical & durability properties in concrete.
- Response Surface Methodology proved its effectiveness as a suitable tool in optimization of concrete performance.

1. Introduction

Worldwide increase in construction works has led to a consequent rise in consumption of cement. The global cement production in the year 1995 was 1.39 billion tons, which increases to 4.1 billion tons in 2022 (Garside 2023). Cement production involves high temperature chemical reactions, often fueled by fossil fuel burning, thereby releasing greenhouse gases (GHG) including substantial amount of carbon dioxide (CO_2) into atmosphere, attributing to global warming and ecological degradation (Worrell et al. 2001). According to statistical data, the cement sector emits 7% of the world's total CO_2 (Deja et al. 2010). The cement industry is therefore, under pressure to reduce its carbon footprint and implement more sustainable practices. There are several initiatives that are being taken worldwide to address this issue. One of the approach that is being adopted globally is the application of alternative raw materials, such as biomass, waste materials, or industrial byproducts in order to develop low-carbon cements that can replace traditional Portland cement partially. In addition to reducing the ecological effect of cement manufacture, continuous efforts are also being undertaken for lessening the production cost and to enhance its quality for achieving higher strength and durability (Balagopal and Viswanathan 2020).

Blended cements, also known as composite cements, are an effective way for lessening the manufacturing cost of Ordinary Portland cement (OPC) while improving its properties (workability, strength and durability properties etc.) and lowering the ecological effect of cement production. The replacement materials used in blended cements are typically latent hydraulic components, such as pozzolanic components like fly ash, burnt clay, silica fume and other wastes (Newman and Choo 2003; Asha et al. 2003). Hydration of OPC chemically forms calcium silicate hydrate (C-S-H), a solid binder that is crucial for imparting strength as well as durability to concrete. Hydration process produces a byproduct called calcium hydroxide, $Ca(OH)_2$, which is highly alkaline and negatively impact long-term stability and durability of the concrete. Blending of suitable pozzolans during hydration develops additional C-S-H, that lessens the $Ca(OH)_2$ content, and helps to fill concrete pores and make it denser and more impermeable, as a result which concrete's resilience and strength enhances (Golewski 2022;

Dwivedi et al. 2006). The recycling of agricultural waste as an alternative material in cement production not only helps to address the issue of waste management but also contributes to reducing air pollution, improving air quality, and mitigating the associated environmental and health risks caused by open burning of wastes (Madurwar et al. 2014). Moreover, using agricultural waste in cement production can also contribute to sustainable practices by reducing the extraction of non-renewable resources like limestone and clay etc. (Ikeagwuani and Nwonu 2019). Wastes generated from several biomasses such as bamboo, corn, coconut, elephant grass, date palm, olive, rice husk, oil palm, and wheat straw, etc. have been incorporated as supplementary cement materials (Thomas et al. 2021; Balagopal and Viswanathan 2020). In this regard, it is essential to screen different biomass and waste materials for their efficacy as pozzolanic materials. Lemon grass and poultry litter are examples of such materials which have not been evaluated for their potentiality as supplementary cement materials (SCMs) in the literature.

East-Indian Lemon grass (*Cymbopogon flexuosus*), a perennial grass is indigenous to the countries such as India, Sri Lanka, Myanmar and Thailand. Due to its aromatic and therapeutic properties, it is frequently utilized in both culinary and medicinal purposes. It is rich in silica (SiO_2) and other compounds that react with $Ca(OH)_2$ to form cementitious compounds (Madhu et al. 2017; Nur Firdus et al. 2016). This makes lemon grass a viable feedstock for supplementary cementitious material (SCM), but research and practical applications are not as widespread as for other SCMs. In construction engineering application, poultry litter is barely used as a cementitious material. It is a blend of manure, bedding materials, and feathers that is frequently utilized as fertilizer or discarded as waste (Fahimi et al. 2020; Cempa et al. 2022). Limited research exists on its use as a supplementary cementitious material, while some studies have explored its potential as a fuel source and other applications.

Calcination, a thermal treatment technique used in industries and scientific fields, involves heating a solid material at elevated temperatures for elimination of volatile components like water, carbon dioxide, or organic matter, with the desired product obtained in the form of ash with altered properties (Rachniyom et al. 2019; Madrid et al. 2012). Based on our current understanding, pyrolysis was not applied as a means of producing SCMs in existing studies. In this particular research, however, the innovative approach involves introducing pyrolysis as an intermediate step within the production process of SCM. Pyrolysis is the thermal degradation of organic materials, such as wood, crop residues, and agricultural waste, at high temperatures (typically between 400 to 800°C) in an oxygen devoid condition, which produces biochar, bio-oil, and syngas (Bhuyan et al. 2022; Lee et al. 2020).

Response surface methodology (RSM) is a design strategy that utilizes statistical analysis techniques to investigate relationships between variables and their related responses. Primary concept of RSM revolves around identifying the correlation between independent and dependent variables, examining their interactions, as well as achieving optimal responses (Alsanusi et al. 2015). RSM has demonstrated its effectiveness in modeling and optimization across diverse fields. RSM offers a significant benefit in terms of cost-effectiveness, as it reduces the need for numerous experimental trials to assess different parameters and their interactions (Kursat and Ehsan 2017; Bashar et al. 2018). Several design models, such as Central Composite Design (CCD), Box-Behnken etc. are utilized to perform RSM analysis. The utilization of RSM can be beneficial approach in the modeling and optimization of concrete (Chopra et al. 2015).

The review of literature suggests that there are knowledge gaps in the utilization of products from lemon grass and poultry litter as SCMs. This investigation aims to develop calcined biochar from the pyrolyed lemon grass biochar, and ash from poultry litter in the form of SCMs, for substitution of traditional cement in concrete. The elemental and chemical composition of calcined lemon grass biochar, poultry litter ash and OPC were analyzed using Energy Dispersive X-ray Spectroscopy (EDX) and X-ray Fluorescence Spectroscopy (XRF) respectively. Moreover, elemental composition, calorific value, density, kinematic viscosity, and acidity of the pyrolytic bio-oil of lemon grass were determined. The functional groups composition of the bio-oil was evaluated by performing Fourier Transform Infrared Spectroscopy (FTIR) technique. Optimization via RSM was performed to quantify the substitution of the prepared SCMs in concrete. Various properties of concrete samples prepared using different weight percentages of SCMs, cured for different time period using various water-cement ratios were evaluated, which includes workability, mechanical properties *viz*. compressive, flexural and split tensile strength, and

durability properties like sulphate resistance and acid resistance. Figure 1 presents the schematic procedure of the preparation of calcined lemon grass biochar and poultry litter ash, their application of in concrete and optimization using RSM.

2. Materials and methods

2.1 Materials

2.1.1 Calcined lemon grass biochar

East-Indian lemon grass (*Cymbopogon flexuosus*) was collected from a tea garden located at Sonitpur district, Assam, India. Lemon grass was washed to remove the dirt and impurities followed by drying in oven at 110℃ to eliminate moisture. Dried feedstock was then grinded to fine powder and subjected to fast pyrolysis in a fixed bed pyrolyzer (Make: MONTECH Instruments). Lemon grass was pyrolyzed at 500°C with heating rate of 20°C/min for 30 min. Bio-oil and biochar yield from the pyrolysis were found to be 26.90 wt.% and 29.26 wt.% respectively. The obtained bio-oil (LG-BO) can be used as fuel and also varieties of value-added products can be obtained through upgradation and separation processes. Whereas the biochar was utilized as the raw material for calcination. Biochar was calcined at 700°C for 3 hrs with heating rate of 10°C/min in muffle furnace (Model: Lindberg Blue M, Make: Thermo Fisher Scientific). The calcined lemon grass biochar (CLGB) to be used as one of the pozzolanic materials in the current investigation was sieved using 45 µm mesh sieve to get the fineness in the range of cement in accordance with ASTM C311. The yield of CLGB from pyrolysed lemon grass biochar was found to be 39.78%. The bulk specific gravity of CLGB was found to be 2.08. Figure 2 displays the preparation process of CLGB from lemon grass.

2.1.2 Poultry litter ash

Poultry litter was obtained from a poultry farm located nearby Tezpur University, Assam, India. Preceding to its use, poultry litter was dried at 110°C, followed by calcination in muffle furnace (Model: Lindberg Blue M, Make: Thermo Fisher Scientific) at temperature of 700°C with heating rate of 10°C/min for 3 hrs. The yield of poultry litter ash (PLA) from the calcination was about 23.97%, which was sieved to get the final product in the range of 45 µm following ASTM C311. The bulk specific gravity of PLA was found to be 2.26. Figure 3 displays the preparation process of PLA from poultry litter.

2.1.3 Composite of Calcined lemon grass biochar and Poultry litter ash

A composite of the obtained calcined lemon grass biochar and poultry litter ash (CLGB-PLA) was prepared by homogenously mixing 50 wt. % of each of these products. The obtained composite was used as another pozzolan in this study.

2.1.4 Ordinary Portland cement (OPC)

OPC of 53 grade (Birla Gold brand) was utilized as a binder conforming to IS 12269 – 2013, and was blended with the above prepared materials *viz*. CLGB and PLA. The bulk specific gravity of OPC was obtained as 3.12.

2.1.5 Fine Aggregate (FA) and Coarse Aggregate (CA)

Sand with maximum particle size of 4.75 mm was utilized as FA in the construction, possessing bulk specific gravity of 2.62. CA consisted of crushed boulder possessing bulk specific gravity of 2.68, with maximum particle size of 20 mm. Both FA and CA met the specifications outlined in ASTM C33.

2.2 Mixture proportions and fabrication of specimens

Four types of concrete mixes were proposed for the investigation following M25 grade of concrete in accordance to IS: 10262 – 2009. The mixture ratio of cement, FA and CA adopted for M25 grade was 1:1:2. The first mix was control mix, where OPC is the only binder material present along with the other aggregates. The next two types of mixes were prepared by using

the binary blends of (i) OPC and CLGB, and (ii) OPC and PLA. Furthermore, a ternary blend of OPC, CLGB-PLA was used as binder with the other aggregates to prepare another concrete mix. Detailed mixture proportions used for the concrete are shown in Table 1. Cement was replaced by the prepared pozzolans with varying proportions (5%, 10%, 15%, 20%, and 25%), with a total powder content of 420 kg/m^3; and the other ingredients were kept constant. Water to cement ratio (WC ratio) adopted was 0.5. Following these design parameters, three different types of specimens viz. cubes, beams and solid cylinders were fabricated for performing compressive, flexural and split tensile strength respectively.

Table 1
Mix Proportions of different aggregates in concrete

Mixes		Mix Proportions				
		Cement (kg/m^3)	Fine Aggregates (kg/m^3)	Coarse Aggregates (kg/m^3)	Calcined Biochar and Ash (kg/m^3)	Water (kg/m^3)
Control Mix	100% OPC	420	480	1080	0	210
Binary	95% OPC + 5% CLGB	399	480	1080	21	210
	90% OPC + 10% CLGB	378	480	1080	42	210
	85% OPC + 15% CLGB	357	480	1080	63	210
	80% OPC + 20% CLGB	336	480	1080	84	210
	75% OPC + 25% CLGB	315	480	1080	105	210
	95% OPC + 5% PLA	399	480	1080	21	210
	90% OPC + 10% PLA	378	480	1080	42	210
	85% OPC + 15% PLA	357	480	1080	63	210
	80% OPC + 20% PLA	336	480	1080	84	210
	75% OPC + 25% PLA	315	480	1080	105	210
Ternary	95% OPC + 2.5% CLGB + 2.5% PLA	399	480	1080	21	210
	90% OPC + 5% CLGB + 5% PLA	378	480	1080	42	210
	85% OPC + 7.5% CLGB + 7.5% PLA	357	480	1080	63	210
	80% OPC + 10% CLGB + 10% PLA	336	480	1080	84	210
	75% OPC + 12.5% CLGB + 12.5% PLA	315	480	1080	105	210

2.3 Methods for testing and characterization

2.3.1 Material characterization

The characterization of the CLGB, PLA and OPC was performed using EDX and X-ray techniques. EDX (Make: JEOL, Japan, Model: JSM 6390LV) was utilized to assess the elemental composition of CLGB and PLA, while XRF (Make: Malvern Panalytical, Model: Zetium) was employed for determination of the chemical composition of CLGB and PLA along with the OPC.

The elements carbon (C), hydrogen (H) and nitrogen (N) of LG-BO were analyzed in a CHN analyzer according to ASTM D5373 (Make: PerkinElmer, USA, Model: 2400 SERIES 2). Oxygen (O) content was determined by means of difference. Calorific value was determined utilizing bomb calorimeter (Make: Ms. Changsha Kaiyuan Instruments Co. Ltd., Changsha, China, Model: SE–1AC/ML). Density of LG-BO was measured using pycnometer following ASTM D1217, and kinematic viscosity was determined at 40°C using HAAKE Falling Ball Viscometer of Type C in accordance with ASTM D445. The acidity of bio-oil was determined using a pH meter (EUTECH pH510). The functional groups composition of the LG-BO was evaluated by performing FTIR-spectroscopy (Make: Perkin Elmer, Model: FORNTIER IR).

2.3.2 Determination of workability

The workability and consistency of fresh concrete are crucial factors in determining its usability and performance in construction applications. Therefore, fresh property assessments were done to meet the workability requirements of concrete mixes. For that, slump flow analysis was conducted for fresh concrete mixes in accordance with ISO 1920-2. The slump cone used in the study was made up of cast iron of standard height 300 mm, with respective internal diameter of 200 mm and 100 mm at the base and top. It involves filling slump cone with concrete mix, compacting it, and then removing the cone. Height gradient between the top of slumped concrete and the cone's original height is measured and provides the workability and consistency of the concrete. Figure 4 represents the procedure of slump flow test.

2.3.3 Compressive Strength

The evaluation of compressive strength involved the fracture of concrete cubes using a universal testing machine (Model: TUTE – 40T, Make: Testwell Instruments, Maharashtra, India) following IS:516 (1959). The concrete cubes measuring 100 × 100 × 100 mm with maximum aggregate size less than 20 mm were prepared, kept in water for 28 days after being cast for 24 hours. Figure 5 demonstrates the process of determination of compressive strength in universal testing machine (UTM). The calculation of compressive strength value for each sample was done as described by Eq. (1):

Compressive Strength = $\frac{P}{A}$ (N/mm^2) (1)

Where, P = Ultimate compressive load, N

A = Surface area, mm^2

2.3.4 Flexural Strength

Flexural or bending strength, is the mechanical property that determines the capacity of material to withstand bending stress without breaking or failing. It was determined by performing three-point bending test following IS:9399 (1979), where the specimen was supported at two points while a load is applied at the center, causing the specimen to bend. The concrete beams for this test were prepared with dimensions measuring 100 × 100 × 500 mm, kept in water for 28 days after being cast for 24 hours, and crushed using UTM (Model: TUTE – 40T, Make: Testwell Instruments, Maharashtra, India). Figure 6 displays the process of determination of flexural strength of the beams in universal testing machine. The calculation of compressive strength value for each sample was done according to Eq. (2):

Flexural Strength = $\frac{3PL}{2bd^2}$ (N/mm^2) (2)

Where, P = Failure load at the midpoint (N)

L = Effective span of the beam (mm)

b = Beam width (mm)

d = Beam thickness (mm)

2.3.5 Split Tensile Strength

Split or indirect tensile strength, involves measuring of tensile strength of a specimen. It was determined by applying a compressive force diametrically to a cylindrical shaped specimen by following IS:5816 (1999). The axial compressive force is exerted parallel to the specimen's axis, leading it to fail under tension along a plane perpendicular to the applied load. The solid cylinders (length = 100 mm, diameter = 200 mm) were prepared, subjected to 28 days water curing, and crushed using UTM (Model: TUTE – 40T, Make: Testwell Instruments, Maharashtra, India). Figure 7 illustrates the process of split tensile strength determination in UTM. The calculation of split tensile strength value for each sample was done as described by Eq. (3):

Split Tensile Strength = $\frac{2P}{\pi DL}$ (3)

Where, P = Maximum Load (N)

D = Cylinder diameter (mm)

L = Length of the line of contact of cylinder (mm)

2.3.6 Sulphate Resistance

Suphate resistance test was conducted according to the specifications outlined in ASTM C1012-04 in order to assess the extent of sulphate detoriation on specimens when submerged in a sulphate solution. The original weight of the cubes was determined after curing, and immersed in water solution containing 5% dissolved magnesium sulphate ($MgSO_4$) for durations of 28 and 56 days (Fig. 8a). Afterward, the samples are removed from the solution, surface dried (Fig. 8b), and determined the final weight. After the removal, a deposit with a white coloration was observed on the concrete surface. Lastly, compression test is performed on the cube samples.

2.3.7 Acid Resistance

Acid resistance test was conducted following the guidelines of ASTM C1898-20 to evaluate the effects of acid exposure on solidified concrete within an acidic solution. After curing, the specimens were removed from water, dried for 24 hours, and then weighed. Weight obtained was considered as the initial weight for further analysis. For execution of this test, two acid solutions of 5% hydrochloric acid (HCl) and 5% sulphuric acid (H_2SO_4) were prepared and diluted to obtain pH level of approximately 2. Subsequently, the concrete cubes were submerged into acid solutions for a duration of 28 and 56 days (Fig. 9a). To ensure consistent concentration, the acid solutions were periodically checked and adjusted once a week. The concrete cubes were then removed from the solutions after 28 and 56 days, respectively (Fig. 9b). Following the removal of the cubes from the acid solutions, they were washed to eliminate unstable particles that were leached due to the acid exposure. Subsequently, the cubes were weighed again to get the final weight and then subjected to compression test.

2.4 Response Surface Methodology (RSM) modelling and optimization

The interrelation between process variables, namely biochar ash (%) i.e. CLGB and PLA composition in concrete, curing period and WC ratio; with the response variable i.e. compressive strength (N/mm^2) was evaluated using CCD with second-order polynomial equation (Eq. 4) in RSM utilizing the Design Expert software (Version 13). CCD was employed for its efficiency in performing a limited sets of experiments and also allow to apply of a second-order model to predict accurately and validate the equation that represents the model.

$$Y = \beta_O + \sum_{i=1}^{k} \beta_i \bullet x_i \sum_{i=1}^{k} \beta_{ii} \bullet x_i^2 + \sum_{i \le j}^{k} \sum_{j} \beta_{ij} \bullet x_i \bullet x_j + \cdots + e$$

4

Where, Y = Predicted response variable, β_o = Regression coefficient, k = Number of factors, e = Random error

Table 2 displays the considered factors and their ranges, while Table 8 illustrates CCD for the experiment. Both graphical and numerical depictions were conducted, and analysis of variance (ANOVA) was performed to assess the statistical significance of regression coefficient. The significance of model terms was determined based on $P < 0.05$. Additionally, the model's fitness was evaluated by calculating the "lack of fit." Three-dimensional (3D) response surface plots were generated to investigate the impact of the parameters and their interaction effects. Furthermore, Design Expert tool was utilized to evaluate the optimum process conditions for achieving maximum compressive strength.

Table 2
Process parameters and their levels considered for RSM

Coded factors	Factors	Experimental Levels		
		-1	0	+1
A	Biochar Ash (%)	10	15	20
B	Curing Period (Days)	21	24.5	28
C	Water-Cement Ratio	0.40	0.50	0.60

3. Results and Discussion

3.1 Material characterization

Table 3 illustrates the elemental analyses performed using EDX, indicated the presence of various elements within samples CLGB, PLA, and CLGB-PLA. In all the samples, the primary element detected was silicon (Si), while traces of other elements, including calcium (Ca), aluminum (Al), and iron (Fe), were also identified. Among the three samples, CLGB-PLA displayed the highest Si content (53.45 wt. %).

Table 3
Elemental compositions of CLGB, PLA and CLGB-PLA

Material	Elements weight (%)										
	Na	Mg	Al	Si	P	S	K	Ca	Mn	Fe	Sum Total
CLGB	0.73	3.38	5.35	47.08	3.33	3.45	25.87	5.13	1.58	4.11	100
PLA	0.56	1.62	0.33	28.15	9.43	4.05	50.37	3.03	1.63	0.82	100
CLGB-PLA	0.62	3.54	2.75	53.45	2.58	2.84	23.52	5.32	1.99	3.38	100

Table 4 displays the chemical constituents of OPC, CLGB, PLA and CLGB-PLA. The oxides of Si, Ca, and Al were found as the major constituents in OPC with small traces of Fe_2O_3 and MgO. While CLGB, PLA and CLGB-PLA composed mainly of SiO_2, CaO, MgO, and K_2O and small traces of Fe_2O_3 and Al_2O_3. The sum of SiO_2, Fe_2O_3, and Al_2O_3 in CLGB and PLA were found to be higher than 50% and that resembles the Class C pozzolan. Whereas, the composition of SiO_2, Fe_2O_3, and Al_2O_3 in CLGB-PLA was greater than 70%, which is similar to the properties to the Class F pozzolan (ASTM C610, 2008). The CLGB-PLA containing SiO_2, Al_2O_3, and Fe_2O_3 of 79.49%, surpasses the value of 70%, set by ASTM C618 for pozzolanic materials.

Table 4
Chemical compositions of OPC, CLGB, PLA and CLGB-PLA

Material	Oxides weight (%)												
	SiO_2	Al_2O_3	Fe_2O_3	MnO	MgO	CaO	Na_2O	K_2O	TiO_2	P_2O_5	SO_3	LOI	Sum Total
OPC	33.62	15.56	4.16	0.048	2.07	37.78	0.13	1.09	1.18	0.22	1.80	2.35	100
CLGB	51.79	2.64	1.15	0.36	3.78	5.73	0.37	21.49	0.14	3.49	3.68	5.38	100
PLA	46.78	2.44	1.26	0.220	7.14	8.42	3.01	9.54	0.18	15.61	3.91	1.50	100
CLGB-PLA	77.82	1.02	0.65	0.144	2.51	3.38	0.90	4.79	0.01	6.19	1.89	0.70	100

The elemental analyses, HVV, and other properties of LG-BO are presented in Table 5. The C, H, N and O content of LG-BO were found to be 54.78%, 7.67%, 0.53% and 37.02%, respectively. The HHV of the LG-BO was determined as 30.24 MJ/kg, which is lesser than diesel's HHV, since O content of LG-BO was significantly higher than diesel (Choudhury et al. 2021). The high O content makes bio-oil appropriate towards catalytic steam reforming attributes to hydrogen energy production. Lower percentage of nitrogen suggested that formation of lesser NO_x gases during combustion (Dhande et al. 2021). The H/C and O/C ratios of LG-BO are 1.68 and 0.50 respectively, which resemble to that of petroleum products (H/C ratio :1.5 to 2.0 and O/C ratio < 0.6) (Choudhury et al. 2021). Calorific value, density, and viscosity etc. are regarded as standard assets for many combustion implementations. The kinematic viscosity of LG-BO was found to be highly viscous than diesel fuel (Wongkhorsub and Chindaprasert 2013), but comparatively lower than the other bio-oils. Therefore, LG-BO necessitates additional treatment to achieve relatable viscosity to diesel; however, it can directly be utilized as furnace oil. The high density value of LG-BO *viz.* 1017 kg/m^3 specified the heavy fractions availability. Table 5 compares LG-BO properties with those produced from *Tithonia diversifolia* (Bhuyan et al. 2022) and coir pith (Choudhury et al. 2021).

Table 5
Comparison of physical and chemical properties of LG-BO with previous findings

Properties		Unit	Bio-oil		
			LG-BO	T. diversifolia (Bhuyan et al. 2022)	Coir pith (Choudhury et al. 2021)
pH		-	4.39	4.63	3.47
Density		kg/m^3	1017	1038	1038
Kinematic Viscosity, 40°C		cSt	25.1	52	53
Elemental composition	C	%	54.78	48.15	60.31
	H		7.67	7.33	9.05
	N		0.53	1.32	2.65
	O[a]		37.02	43.20	27.99
Calorific value		MJ/kg	30.24	26.88	28.38
H/C molar ratio		-	1.68	1.94	1.80
O/C molar ratio		-	0.50	0.56	0.348

[a]Calculated from difference

Figure 10 illustrates FTIR spectrum of LG-BO. The broad O–H absorption peak at 3450 cm^{-1} shows the availability of phenolic and alcoholic compounds (Lu et al. 2008). The existence of methylene groups in LG-BO was specified by the peak at 2920 cm^{-1} (Çulcuoglu et al. 2005). The C = C stretching vibration due to absorption at 1638 cm^{-1} indicates the alkenes and aromatic compounds. The bending vibration peak at 1387 cm^{-1} indicates C–H group of alkanes (Demiral et al. 2008). The O–H bending and C–O stretching resulted in the absorbance peaks within the range of 1300 and 900 cm^{-1}, which shows the existence of primary, secondary, and tertiary alcohols along with phenols (Lu et al. 2008).

3.2 Engineering properties of concrete

3.2.1 Concrete workability

The concrete mixtures and their slump properties were presented in Table 6. The control mix concrete exhibited the highest slump of 60 mm, indicating a shear type of slump. With the addition of CLGB and PLA in the mixture, the slump values demonstrated a decrease. By increasing the percentage of CLGB and PLA up to 25%, the slump values reduced up to 25 mm for CLGB mix and 20 mm for PLA mix respectively, showing true slump property which represents stiff, consistent and no workability. The workability of concrete prepared with the incorporation of CLGB and PLA up to 15% found to be within the medium range (50–100 mm), exhibiting shear slump properties.

Table 6
Slump characteristics of the concrete mixtures

Concrete mix	Slump (mm)	Type of slumps
OPC (100%)	60	Shear
CLGB (5%) + OPC (95%)	60	Shear
CLGB (10%) + OPC (90%)	55	Shear
CLGB (15%) + OPC (85%)	50	Shear
CLGB (20%) + OPC (80%)	45	True
CLGB (25%) + OPC (75%)	25	True
PLA (5%) + OPC (95%)	55	Shear
PLA (10%) + OPC (90%)	50	Shear
PLA (15%) + OPC (85%)	50	Shear
PLA (20%) + OPC (80%)	30	True
PLA (25%) + OPC (75%)	20	True

Theoretically, increasing the water content in the concrete mix can enhance workability but may also lead to potential issues such as segregation, bleeding, drying shrinkage etc., which reduces concrete's strength and durability. However, pozzolanic material functions as a proficient water absorbent. Consequently, adding pozzolanic material to the concrete mix can decrease the water content and subsequently affect its workability. Despite the reduction in workability, additional tests including compressive, flexural, and split tensile strength were studied upon the inclusion of SCMs.

3.2.2 Compressive strength

The compressive strength test revealed varying strengths of the specimens for different levels of CLGB and PLA substitution. Table 7 presents the compressive strength for different concrete mixes. The compressive strength achieved after 28 days ranges from 27.22 N/mm^2 to 34.06 N/mm^2 for different concrete mixes. Figure 11 shows different compressive strength values corresponding to the replacement percentage of SCMs. Among all the concrete, the ternary blend concrete (CLGB-PLA-

OPC) demonstrated the highest compressive strengths, ranging from 33.12 N/mm^2 to 34.06 N/mm^2 for a replacement percentage of 10–20% after the curing of 28 days.

Table 7
Mechanical properties of the CLGB-PLA, CLGB and PLA mixed concrete

Blend			Compressive Strength (N/mm^2)		Flexural Strength (N/mm^2)		Split Tensile Strength (N/mm^2)	
			21 Days	28 Days	21 Days	28 Days	21 Days	28 Days
Control Mix	OPC	100% OPC	31.35	33.62	6.95	8.54	2.58	3.10
Binary	CLGB + OPC	95% OPC + 5% LGA	30.18	32.17	7.18	8.48	2.31	2.87
		90% OPC + 10% LGA	31.24	33.74	7.02	8.63	2.66	3.04
		85% OPC + 15% LGA	30.67	32.27	6.87	8.50	2.35	2.79
		80% OPC + 20% LGA	27.84	29.18	6.97	8.33	2.18	2.69
		75% OPC + 25% LGA	25.13	27.88	6.43	7.96	2.18	2.57
	PLA + OPC	95% OPC + 5% PLA	28.44	30.08	6.61	7.63	2.43	2.80
		90% OPC + 10% PLA	28.83	31.26	6.61	7.80	2.61	2.85
		85% OPC + 15% PLA	27.62	29.87	6.42	7.74	2.52	2.78
		80% OPC + 20% PLA	26.83	28.38	6.02	7.57	2.38	2.74
		75% OPC + 25% PLA	25.17	27.22	6.15	7.57	2.33	2.74
Ternary	CLGB + PLA + OPC	95% OPC + 2.5% LGA + 2.5% PLA	29.77	32.43	7.13	8.54	2.23	2.91
		90% OPC + 5% LGA + 5% PLA	31.12	33.90	7.10	8.91	2.68	3.10
		85% OPC + 7.5% LGA + 7.5% PLA	32.20	34.06	8.06	9.19	2.64	3.16
		80% OPC + 10% LGA + 10% PLA	31.68	33.12	7.35	8.63	2.37	2.98
		75% OPC + 12.5% LGA + 12.5% PLA	29.63	31.35	6.98	8.45	2.13	2.87

The presence of high silica (SiO_2) in CLGB and PLA was identified as the sole contributing factor to the enhanced compressive strength. This resulted in the development of supplementary C-S-H compounds, indicating filling of the voids of concrete. Furthermore, the fine particle size of calcined biochar and ash played a role in reducing air content by filling the pores, thereby increasing the unit weight of concrete, which tends to exhibit improved strength (Golewski 2022; Dwivedi et al. 2006).

3.2.3 Flexural Strength

During flexural strength determination, control mix concrete failed abruptly, while the concrete specimens containing CLGB and PLA exhibited a ductile behavior, providing ample warning. Table 7 displays the flexural strength values of different concrete mixtures. Among them, the concrete specimen containing 15% CLGB-PLA achieved the highest flexural strength of 9.19 N/mm^2 after 28 days of curing. For the binary blend cement, the maximum flexural strengths were 8.63 N/mm^2 and

7.80 N/mm^2, observed in the concrete specimens with 10% CLGB and 10% PLA, respectively. The outcomes show that the trend of reaching maximum flexural strength varies depending on the concrete mixes used. Notably, the flexural strength value of the concrete specimen containing 15% CLGB-PLA (9.19 N/mm^2) significantly exceeds that of the control mix concrete (8.54 N/mm^2) after 28 days of curing. Figure 11 displays change in the flexural strength values corresponding to alter in substitution percentage of SCMs.

3.2.4 Split Tensile Strength

The split tensile strength results of different concrete mixtures are included in Table 7. Out of these, the concrete specimen with 15% CLGB-PLA exhibited maximum split tensile strength of 3.16 N/mm^2 at 28 days. For binary blend, specimens having 10% CLGB and 10% PLA showed maximum split tensile strengths of 3.04 and 2.85 N/mm^2, respectively. The split tensile strength of the concrete with 15% CLGB-PLA (3.16 N/mm^2) significantly surpassed that of the control mix concrete (3.10 N/mm^2) at 28-day curing period. Figure 11 demonstrates different split strength values corresponding the replacement percentage of SCMs.

3.2.5 Correlation of compressive strength with flexural and split tensile strength

A strong and positive linear correlation was observed between compressive strength with both flexural as well as split tensile strength of concrete specimens cured for 28 days, as depicted in Fig. 12. The correlation analysis yielded Pearson's coefficients of correlation (r^2) of 0.8801 and 0.9010 between compressive and flexural strength, and between compressive and split tensile strength. This signifies that flexural and split tensile strength can be accurately evaluated based on the obtained compressive strength values applying the equations 5 and 6:

$y_1 = 1.884x + 2.3872$ (5)

$y_2 = 0.0573x + 1.1157$ (6)

Where, y_1 is the flexural strength (N/mm^2), y_2 is the split tensile strength (N/mm^2) and x is the compressive strength (N/mm^2).

According to Zady (2000), a robust association exists between two variables when the Pearson's coefficient of correlation falls within the range of 0.7 to 1. This finding aligns with the results obtained in the current study, therefore, the obtained correlation values indicate a strong relationship between these variables.

3.3 Statistical analysis and design of experiments using RSM

RSM was employed to achieve a practical model between the studied variables and the experimental response i.e. the compressive strength (N/mm^2) of ternary blended CLGB-PLA concrete. The RSM process optimization using CCD, involving 20 experimental runs with 3 process variables and 1 response variable were presented in Table 8. The process variables included the substitution percentage of CLGB-PLA named as biochar ash (%), curing period (day), and WC ratio. During the experiments, the concrete specimens demonstrated excellent results (Table 7) for 10–20% biochar ash replacement during 28 days curing period. Based on these findings, the ranges considered for the process variables were as follows: Biochar ash (10–20%), curing period (21–28 days), and WC ratio (0.40–0.60). The second-order polynomial equation describing the comprehensive interaction among the independent variables are presented in equations 7 and 8 with coded and actual factors respectively.

Compressive Strength = + 33.74 + 0.6310 × A + 0.7730 × B + 0.4480 × C – 0.2787 × AB – 0.0937 × AC + 0.3213 × BC – 1.36 × A^2 – 0.5614 × B^2 – 0.4764 × C^2 (7)

$$\text{Compressive Strength} = -23.48589 + 2.24384 \times \text{Biochar Ash} + 2.24631 \times \text{Curing Period} + 32.44136 \times \text{Water-cement ratio} - 0.015929 \times \text{Biochar Ash} \times \text{Curing Period} - 0.187500 \times \text{Biochar Ash} \times \text{Water-cement ratio} + 0.917857 \times \text{Curing Period} \times \text{Water-cement ratio} - 0.054455 \times \text{Biochar Ash}^2 - 0.045826 \times \text{Curing Period}^2 - 47.63636 \times \text{Water-cement ratio}^2 \quad (8)$$

Table 9 provides an overview of the ANOVA findings, where F-tests were used to examine the statistical model. As indicated by $p < 0.05$ and F-value of 250.71, the analysis demonstrated that both the regression as well as the model itself exhibit statistical significance at 95% level of confidence. The probability of occurrence of high F-value for the model attributed towards noise is 0.01. The terms A, B, C, AB, BC, A^2, B^2, and C^2 are significant, while among the individual parameters, curing period has the highest significance followed by biochar ash and WC ratio. The non-significance of "lack of fit" with *F*-value of 4.33, direct towards the model's fitness. The noise can be a probable cause for such high *F*-value of "lack of fit" with 6.67% probability. The adjusted R^2 and predicted R^2 were found to have strong agreement with model's R^2 value of 0.9956. The signal-to-noise ratio of 50.866 (greater than desired value of 4) signifies the adequate precision. The coefficient of variance (CV) value if less than 10%, designates reproducible models (Zhou et al. 2018). In this analyses, CV for the compressive strength obtained was 0.39%, which confirms the reproducibility of the model. Figure 13 illustrates the relationship amongst predicted and actual compressive strengths. The position of both the predicted and actual values were very close to the diagonal line, which signifies a strong correlation between them. It establishes a graphical validation that ANOVA generated regression model equation can efficiently express the interaction of independent variables and compressive strength.

Table 8
CCD experimental design matrix

Sl. No.	Biochar Ash (%)	Curing Period (Days)	Water – Cement Ratio	Experimental Compressive Strength (N/mm^2)	Predicted Compressive Strength (N/mm^2)
1	15	21	0.50	32.20	32.41
2	15	24.5	0.50	33.65	33.74
3	20	28	0.40	31.80	31.79
4	10	21	0.60	29.90	29.88
5	15	28	0.50	34.06	33.95
6	15	24.5	0.50	33.85	33.74
7	20	24.5	0.50	33.01	33.01
8	10	28	0.40	30.90	30.90
9	20	21	0.60	31.54	31.51
10	10	24.5	0.50	31.65	31.75
11	20	28	0.60	33.06	33.14
12	10	21	0.40	29.55	29.44
13	20	21	0.40	31.50	31.45
14	15	24.5	0.50	33.73	33.74
15	10	28	0.60	32.60	32.63
16	15	24.5	0.50	33.78	33.74
17	15	24.5	0.40	32.65	32.82
18	15	24.5	0.60	33.78	33.71
19	15	24.5	0.50	33.85	33.74
20	15	24.5	0.50	33.80	33.74

Table 9
ANOVA analysis of the model

Source	Sum of Squares	df	Mean Square	F-value	p-value prob > *F*	
Model	35.54	9	3.95	250.71	< 0.0001	significant
A- Biochar Ash	3.98	1	3.98	252.79	< 0.0001	
B-Curing Period	5.98	1	5.98	379.37	< 0.0001	
C-Water/Cement Ratio	2.01	1	2.01	127.43	< 0.0001	
AB	0.6216	1	0.6216	39.47	< 0.0001	
AC	0.0703	1	0.0703	4.46	0.0608	
BC	0.8256	1	0.8256	52.42	< 0.0001	
A^2	5.10	1	5.10	323.58	< 0.0001	
B^2	0.8666	1	0.8666	55.02	< 0.0001	
C^2	0.6240	1	0.6240	39.62	< 0.0001	
Residual	0.1575	10	0.0158			
Lack of Fit	0.1280	5	0.0256	4.33	0.0667	not significant
Pure Error	0.0295	5	0.0059			
Cor Total	35.70	19				
R^2 = 0.9956, adjusted R^2 = 0.9916, predicted R^2 = 0.9726, Std. Dev. = 0.13, C.V. = 0.39%						

3.3.1 Response plots

Figure 14 presents the 3D response surfaces showcasing individual and synergistic effects of factors on compressive strength of CLGB-PLA mix concrete. The surface plot showing the synergistic influence of biochar ash and curing period on compressive strength is represented in Fig. 14 (a). The compressive strength is higher when OPC is replaced by biochar ash i.e. CLGB-PLA ranging between 14–18% wt., with the curing period exceeding 25 days. But the compressive strength is low beyond that range of replacement, even at the maximum curing period of 28 days. This phenomenon can be explained by considering the optimal interaction between SiO_2 in CLGB-PLA and $Ca(OH)_2$ in concrete mix, which enhances the development of additional C-S-H and in turn maximizes the compressive strength. The maximum strength of 34.06 N/mm^2 was obtained at 15% replacement and curing period of 28 days. For the replacement percentage below 14% wt., amount of SiO_2 is insufficient to react effectively with $Ca(OH)_2$, whereas replacements beyond 18% wt. yielded enhanced SiO_2 content but lack the required $Ca(OH)_2$ for development of adequate C-S-H in concrete. Consequently, this leads to decline of the compressive strength.

The combined effect of biochar ash i.e. CLGB-PLA (%) and water-cement ratio is demonstrated in Fig. 14 (b). The plot showed a compressive strength of 29.55 N/mm^2 at the lower level of both biochar ash replacement and WC ratio, which increased to 32.60 N/mm^2 by increasing WC ratio up to 0.60. A compressive strength of 33.06 N/mm^2 could be observed when the biochar ash replacement was increased to 20% wt. and WC ratio to 0.60. Maximum compressive strength of 34.06 N/mm^2 was attained at 15% biochar ash replacement and WC ratio of 0.50. This could be attributed to the fact that when WC ratio was at low level, the amount of water in the concrete was less, which hindered the effective interaction of water medium with both biochar ash and OPC, creating an adverse effect on compressive strength. Conversely, when WC ratio became too

high, the biochar ash absorbed more water, led to reduction in strength because of the appearance of the reduction and bleeding phenomena, and inadequate distribution of the aggregates within the mixture. This resulted in the retention of significant amount of water inside the concrete mixture, that evaporated gradually and a number of holes are formed after concrete hardening which in turn reduced the concrete strength significantly. Figure 14 (c) illustrates the impact of curing period and WC ratio on compressive strength. The curing period shows higher effect on compressive strength with greater WC ratio than at lower WC ratio. The compressive strength is observed to be more dependent on curing period compared with WC ratio as can be seen from the slope of the curing period. With increase in WC ratio, the incremental increase in compressive strength is low. The plot showed a compressive strength of 29.55 N/mm^2 at the lower level of both WC ratio (0.40) and curing period (21 days), which increased to 31.80 N/mm^2 by enhancing curing period up to 28 days. A maximum of 33.06 N/mm^2 of compressive strength could be observed when WC ratio is increased to 0.60 and curing period to 28 days.

3.3.2 Model optimization and validation

Using Design Expert tools, the regression equation was solved to determine the optimal conditions of the specified parameters. A total of 15 solutions with a desirability of 1.00 were identified, amongst which the predicted optimal condition to achieve maximum compressive strength in the concrete was biochar ash (CLGB-PLA) percentage of 17.57%, curing period of 25.82 days, and water-cement ratio of 0.54. This combination of parameters is expected to result in a compressive strength of 33.99 N/mm^2. Triplicate experiments were conducted under the specified optimal condition, and the average compressive strength obtained was 33.94 ± 0.12 N/mm^2. This value closely matched the predicted value, indicating a strong agreement between the experimental results and the anticipated outcome.

In addition, the compressive strength value obtained from the aforementioned optimum conditions was used to evaluate flexural as well as split tensile strength. These calculations were performed following the equations obtained in the Pearson's correlation analysis. The flexural and split tensile strength stood in 8.78 ± 0.02 N/mm^2 and 3.06 ± 0.02 N/mm^2 respectively. Furthermore, the concrete specimens prepared following the RSM-based optimal conditions were used in the evaluation of the durability properties viz. sulphate resistance and acid resistance of the concrete.

Acid resistance

Acid resistance test involved immersing concrete cube specimens in 5% hydrochloric acid (HCl) and 5% sulfuric acid (H_2SO_4) solutions for 28 and 56 days respectively, and thereafter, the changes in weight as well as strength were observed. Triplicate experiments were performed for each sample. The test results revealed that among the two acid solutions, all the concrete specimens were highly affected by the HCl solution resulting in higher weight loss and strength. Additionally, the cube made from the control mix demonstrated a greater susceptibility to both the acid solutions in comparison to the CLGB-PLA blended cube. This disparity is attributed towards the creation of calcium chloride (CaCl) and calcium sulphate ($CaSO_4$), specifically soluble salts, through the interaction of HCl and H_2SO_4 with cement. This reaction is particularly pronounced when calcium-containing fillers are present. The higher concentration of calcium facilitates the absorption of more hydrochloric acid by OPC (Bassuoni et al. 2007; Kannan and Ganesan 2014). An additional factor contributing to the decline in weight and strength was the leaching of primary hydrated components like calcium, silica, and alumina due to the acidic nature of both HCl and H_2SO_4 solutions, which led to deterioration (Siad et al. 2010). The test results revealed that percentage of weight reduction varies from 8.4 to 11.12 and 20.27 to 23.44, whereas strength loss (%) was observed between 11.37 to 14.90 and 23.60 to 28.17, respectively for 28 days and 56 days in 5% HCl solution. On the other hand, the weight loss percentage was observed between 6.80 to 9.27 and 13.03 to 19.38, while strength loss (%) varies from 9.55 to 12.32 and 16.26 to 24.49, respectively for 28 days and 56 days in 5% H_2SO_4 solution.

These results suggest that the CLGB-PLA mix concrete specimens prepared following the optimal conditions from RSM exhibit higher resistance towards acidic environment. Moreover, both the concrete samples have experienced higher damage by HCl treatment over H_2SO_4. Table 10 displays the detailed information on compressive strength and weight loss of specimens.

Table 10
Reduction in weight and compressive strength of concrete cubes due to acid attack

Weight Loss (g)					
Mix	Weight after curing period (g)	5% HCl Acid Solution		5% H_2SO_4 Acid Solution	
		28 days	56 days	28 days	56 days
Control mix	2414.43 ± 0.06 (28 days)	2145.81 ± 0.16	1848.43 ± 0.15	2190.48 ± 0.33	1946. 50 ± 0.24
CLGB-PLA mix	2422.92 ± 0.10 (25.82 days)	2208.62 ± 0.14	1931.70 ± 0.20	2258.12 ± 0.23	2107.07 ± 0.08
Compressive Strength (N/mm^2)					
Mix	Compressive strength after curing period (g)	5% HCl Acid Solution		5% H_2SO_4 Acid Solution	
		28 days	56 days	28 days	56 days
Control mix	33.68 ± 0.09 (28 days)	28.66 ± 0.10	24.19 ± 0.17	29.53 ± 0.10	25.43 ± 0.08
CLGB-PLA mix	33.94 ± 0.12 (25.82 days)	30.08 ± 0.07	25.93 ± 0.05	30.70 ± 0.09	28.42 ± 0.13

Sulphate resistance

Sulphate attack on concrete structure can cause possible expansion, cracking, loss of strength and disintegration in it. When the concrete comes in contact with sulphate atmosphere, the sulphate ions react with the calcium-aluminate-hydrate (C-A-H) and $Ca(OH)_2$ available in concrete and results in two products *viz.* ettringite and gypsum. Ettringite increases the solid volume of the structure, which leads to expansion, fracture and weight loss, whereas gypsum softens the concrete as well as reduction in strength and weight (Prithiviraj et al. 2022). Table 11 displays the strength and weight reduction of specimens due to sulphate attack. The weight loss (%) occurs in the range of 0.84 to 2.28 and 0.29 to 2.82, whereas the strength loss (%) varies from 3.89 to 6.89 and 12.05 to 15.52, respectively for 28 and 56 days. The findings of the experiments showed that the CLGB-PLA mix concrete offered less weight loss as well as strength loss compared to control one. This was probably due to the development of additional C-S-H due to reaction of SiO_2 in CLGB-PLA with $Ca(OH)_2$ in concrete, resulting in inaccessibility of $Ca(OH)_2$ to combine with sulphate ions to produce ettringate; and also reduce the permeability that helps in penetration of the sulphate ions into the concrete (Ramezanianpour and Hooton 2013; Juenger and Siddique 2015). Since, the control mix concrete was more permeable in nature due to absence of additional fillers, more sulphate ions penetrated into it and resulting in loss of strength and weight. Another reason of higher aggressiveness of $MgSO_4$ solution towards control mix concrete was because of the dissolving of C-S-H and C-A-H compounds by sulphate (Al-Attar and Taha 2018).

Table 11
Reduction in weight and compressive strength of concrete cubes due to sulphate attack

Weight Loss (g)			
Mix	**Weight after curing period (g)**	**5% $MgSO_4$ Acid Solution**	
		28 days	**56 days**
Control mix	2414.43 ± 0.06 (28 days)	2359.37 ± 0.51	2346.20 ± 0.15
CLGB-PLA mix	2422.92 ± 0.10 (25.82 days)	2402.34 ± 0.21	2395.32 ± 0.26
Compressive Strength (N/mm^2)			
Mix	**Compressive strength after curing period (g)**	**5% $MgSO_4$ Acid Solution**	
		28 days	**56 days**
Control mix	33.68 ± 0.09 (28 days)	31.36 ± 0.24	28.45 ± 0.46
CLGB-PLA mix	33.94 ± 0.12 (25.82 days)	32.62 ± 0.30	29.85 ± 0.26

3.4 Comparative analysis on the utilization percentage of the prepared bio-based material with earlier investigation

Table 12 presents the comparison of the current study and few existing literatures that focused on the utilization of bio-based products as SCMs. The collected data reveals that the bio-based products were used within the replacement percentage ranges from 0.5 to 40%, where maximum compressive strength was obtained within the range of 1 to 10% replacement for most of the studies. Figure 15 displayed the correlation between compressive strength and different replacement percentage of various bio-based products. Around 70% of the studies are based on the binary blends exhibiting optimum replacement up to 15%. In contrast, the remaining 30% of the studies have utilized ternary blends with an optimum substitution up to 20%. However, they show lower compressive strength in comparison to current research (17.57% of CLGB-PLA replacement) for the equivalent M25 concrete grade. Figure 16 displays the comparison of compressive strength of different binary and ternary blended concrete.

Table 12
Comparative analysis of replacement percentage of bio-based products from existing research

Combination		Water-cement ratio	Concrete Grade	Compressive Strength (N/mm^2)	Utilization range of pozzolans (%)	Optimum pozzolans (%)	Reference
Binary	Ternary			28 Days			
C + BLA		0.50	M15	12.67–28.56	10–40	10	Olutoge and Oladunmoye 2017
C + BLA		-	M15	16.50–23.13	5–20	5	Umoh and Ujene 2014
C + BLA		-	M20	12.30–18.60	5–15	5	Asha et al. 2014
C + BSA		0.60	M15	22.88	5–30	10	Ikeagwuani et al. 2019
C + BLA		0.60	M15	12.93–16.98	5–15	10	Ademola and Buari 2014
C + BLA		0.50	M15	12.74–14.67	5–20	5	Olofintuyi et al. 2015
C + BNLA		-	M30	19.72–30.13	15–25	15	Pawar and Khaire 2018
C + BNLA		-	M30	33.44	15	15	Musthafa et al. 2019
			M35	39.42			
			M40	44.62			
C + BNSF		0.45	M25	18.91–35.55	0.5–2.5	1	Chandar et al. 2018
C + BNSA		0.45	M30	28.26–35.03	5–20	10	Paulose and Babu 2021
	C + RHA + CSP	0.45	M25	24.30–28.10	10–35	20	Kumar et al. 2018
C + RHA		-	M25	22.28–25.12	10–20	15	Hussain and Parasuram 2018
C + RHA		-	M20	21.20–29.60	5–25	10	Kumar and Velayutham 2019
C + RHA		-	M20	21.00–31.5	5–15	5	Rao et al. 2014
C + SBA		-	M20	26.43–28.50	5–10	5	Mangi et al. 2017
C + WHA		0.45	M25	22.60–27.12	5–20	15	Abirami et al. 2018

C: Cement, BLA: Bamboo Leaves Ash, BSA: Bamboo Steam Ash, PPA: Plantain Peel Ash, BNLA: Banana Leaves Ash, BNSA: Banana Steam Ash, BNSF: Banana Steam Fiber, CSA: Coconut Shell Ash, RHA: Rice Husk Ash, SBA: Sugarcane Bagasse Ash, WHA: Water Hyacinth Ash, BTA: Bamboo Trunk Ash, GSS: Grinded Snail Shell, SHA: Sorghum husk ash, $CaCl_2$: Calcium Chloride, CSP: Coconut Shell Powder, CFP: Coconut Feather Powder, TW: Tea Waste, FA: Fly Ash

Combination		Water-cement ratio	Concrete Grade	Compressive Strength (N/mm^2)	Utilization range of pozzolans (%)	Optimum pozzolans (%)	Reference
Binary	**Ternary**			**28 Days**			
	C + BTA + GSS	0.50	M15	17.75–18.74	5–15	15	Olofintuyi and Oladapo 2019
C + SBA		-	M25	10.97–26.45	5–20	5	Mahesh et al. 2017
C + PPA		-	M15	25.40–27.60	5–25	5	Ahmad and Ado 2016
C + CSA		0.50	M25	24.59–33.46	5–25	10	Kumar 2020
	C + SHA + $CaCl_2$	0.60	M20	18.13–26.45	5–25	5	Tijani et al. 2020
	C + CSP + CFP	-	-	14.60–16.10	10–30	10	Revathi et al. 2018
	C + TW + FA	0.40	M40	49.77–51.12	5–10	5	Datta et al. 2019
	C + CLGB + PLA	0.54	M25	33.94	5–25	17.57	**This work**

C: Cement, BLA: Bamboo Leaves Ash, BSA: Bamboo Steam Ash, PPA: Plantain Peel Ash, BNLA: Banana Leaves Ash, BNSA: Banana Steam Ash, BNSF: Banana Steam Fiber, CSA: Coconut Shell Ash, RHA: Rice Husk Ash, SBA: Sugarcane Bagasse Ash, WHA: Water Hyacinth Ash, BTA: Bamboo Trunk Ash, GSS: Grinded Snail Shell, SHA: Sorghum husk ash, $CaCl_2$: Calcium Chloride, CSP: Coconut Shell Powder, CFP: Coconut Feather Powder, TW: Tea Waste, FA: Fly Ash

4. Conclusions

The current experimental work aimed to produce novel supplementary cementitious material (SCM) using East-Indian Lemon grass and poultry litter, and to examine mechanical and durability properties of concrete structures fabricated by mixing different percentage of the prepared bio-based SCMs *viz*. CLGB and PLA ranging between 0–25%. Furthermore, RSM was applied for designing the experiment and create a model for the prediction of maximum replacement percentage of the prepared SCM in concrete without affecting the concrete properties. The experiments yielded the following conclusions:

- Pyrolysis of East-Indian Lemon grass yielded 26.90 wt.% bio-oil along with a biochar yield of about 29.26 wt.%. The bio-oil (LG-BO) exhibits a higher calorific value of 30.24 MJ/kg, with H/C and O/C ratios resemble those found in petroleum products. The kinematic viscosity of LG-BO is viscous than diesel fuel, which can be directly utilized as furnace oil.
- Among the prepared SCMs, CLGB-PLA shows that SiO_2, Fe_2O_3 and Al_2O_3 together constitutes 79.49%, resembling the properties of Class F pozzolan in accordance to ASTM C610, 2008 for pozzolanic materials.
- The model generated using 3-factor 3-level RSM-CCD to predict the optimum mechanical and durability performance of the CLGB-PLA mix concrete demonstrates to be significant with strong correlation and predictability. Based on the optimal conditions, the compressive strength value obtained is 33.94 ± 0.12 N/mm², lies very closed to predicted value of 33.99 N/mm². The flexural and split tensile strength obtained are 8.78 ± 0.02 N/mm² and 3.06 ± 0.02 N/mm² respectively.

- The substitution of 17.57% of OPC with CLGB-PLA in concrete results in the enhancement of durability characteristics like acid resistance and sulphate resistance of the concrete structure when immersed in acidic solutions (5% HCl and 5% H_2SO_4) and sulphate solution (5% $MgSO_4$).

Declarations

The authors declare that there is no competing financial interests or personal relationships that could have appeared to influence the work reported in this paper.

Acknowledgements

The first author gratefully acknowledged the financial grant in the form of National Doctoral Fellowship (NDF), from AICTE, New Delhi, India. Authors would also like to thank Assam Kaziranga University, Jorhat, Assam for providing the facility of Universal Testing Machine and SAIC, Tezpur University for providing other analysis facility.

CRediT authorship contribution statement

Neelam Bora: Conceptualization, Methodology, Investigation, Writing - original draft. **Niran Daimary:** Resources, Formal analysis. **Mondita Athparia:** Investigation, Writing - review & editing. **M. K. Loganathan:** Resources, Investigation. **Rupam Kataki:** Visualization, Supervision, Writing - review & editing, Validation, Project Administration.

References

1. Abirami U, Kayalvizhi K, Pavithra K, Govandan A (2018) Experimental Study on Behaviour of Concrete Replaced with Water Hyacinth Ash. Int J Eng Res Technol 6(14):1–3
2. Ademola SA, Buari TA (2014) Behaviour of bamboo leaf ash blended cement concrete in sulphates environment. IOSR J Eng 4(6):1–8
3. Ahmad DA, Ado M (2016) Investigation in to the use of plantain peels ash as an admixture in concrete. Int J Eng Sci Comp 6(5):5377–5380
4. Al-Attar TS, Taha AA (2018) Performance of high-volume fly ash self-compacting concrete exposed to external sulfate attack. In Proceedings of the 6th International Conference on Durability of Concrete Structures, ICDCS, Leeds, UK
5. Alsanusi S, Bentaher L (2015) Prediction of Compressive Strength of Concrete from Early Age Test Result Using Design of Experiments (RSM). Int. J. Civil Environ. Struct. Constr. Archit. Eng. 9(12): 2015
6. Asha P, Salman A, Kumar RA (2014) Experimental study on concrete with bamboo leaf ash. Int J Eng Adv Technol 3(6):46–51
7. Balagopal V, Viswanathan TS (2020) A Comprehensive Exploration on Sustainable Supplementary Cementitious Materials Derived from Agro-Wastes. Int J Eng Adv Technol 9(3):2482–2489
8. Bashar S, Veerendrakumar C, Muhd F (2018) Rubbercrete mixture optimization using response surface methodology. J Clean Prod 171:1605–1621
9. Bassuoni MT, Nehdi M, Amin M (2007) Self-compacting concrete: Using limestone to resist sulfuric acid. Proc. Inst. Civ. Eng. Constr. Mater. 160:113–123
10. Bhuyan N, Narzari R, Baruah SMB, Kataki R (2022) Comparative assessment of artificial neural network and response surface methodology for evaluation of the predictive capability on bio-oil yield of Tithonia diversifolia pyrolysis. Biomass Convers Biorefin 12:2203–2218. https://doi.org/10.1007/s13399-020-00806-x
11. Cempa M, Olszewski P, Wierzchowski K, Kucharski P, Białecka B (2022) Ash from Poultry Manure Incineration as a Substitute for Phosphorus Fertiliser. Mater 15:3023. https://doi.org/10.3390/ma15093023

12. Chandar SP, Gunasekaran K, Nabeel Babu VP, Potti R (2018) Experimental investigation on the mechanical properties of concrete mixed with banana stem fiber as well as hybrid steel fiber. Rasayan J Chem 11(2):640–646. http://dx.doi.org/10.31788/RJC.2018.1123011
13. Chopra P, Kumar RS, Kumar M (2015) Artificial neural networks for the prediction of compressive strength of concrete. Int J Appl Sci Eng 13(3):187–204
14. Choudhury ND, Bhuyan N, Bordoloi N, Saikia N, Kataki R (2021) Production of bio-oil from coir pith via pyrolysis: kinetics, thermodynamics, and optimization using response surface methodology. Biomass Convers Biorefin 11:2881–2898
15. Çulcuoglu E, Ünay E, Karaosmanoglu F, Angin D, Şensöz S (2005) Characterization of the bio-oil of rapeseed cake. Energ Source 27(13):1217–1223
16. Datta M, Gupta A, Dwivedi A, Kosta A (2019) Experimental study of cement replacement with tea waste and flyash. J Emerg Technol Innov Res 6(6):63–68
17. Deja J, Uliasz-Bochenczyk A, Mokrzycki (2010) CO_2 emissions from Polish cement industry. Int J Greenh Gas Control 4(4):583–588
18. Demiral I, Atilgan NG, Şensöz S (2008) Production of biofuel from soft shell of pistachio (Pistacia vera L). Chem Eng Commun 196(1–2):104–115
19. Dhande DY, Sinaga N, Dahe KB (2021) Study on combustion, performance and exhaust emissions of bioethanol-gasoline blended spark ignition engine. Heliyon 7(3)
20. Dwivedi VN, Singh NP, Das SS, Singh NB (2006) A new pozzolanic material for cement industry: Bamboo leaf ash. Int J Phys Sci 1(3):106–111
21. Fahimi A, Bilo F, Assi A et al (2020) Poultry litter ash characterisation and recovery. Waste Manag 111:10–21
22. Garside M (2023) Cement Industry Worldwide. Statista. www.statista.com
23. Golewski GL (2022) The Role of Pozzolanic Activity of Siliceous Fly Ash in the Formation of the Structure of Sustainable Cementitious Composites. Sustain Chem 3:520–534. https://doi.org/10.3390/suschem3040032
24. Hussin TAR, Parasuraman J (2018) Partial replacement of cement with commercial available rice husk ash in concrete. Infrastructure Univ Kuala Lumpur Res J 6(1):1–9
25. Ikeagwuani CC, Nwonu DC, Obetule DA, Omeje MU, Festus T (2019) Potential of bamboo stem ash as supplementary cementitious material in concrete production. Int J Eng Res Technol 8(8):75–80
26. Juenger MCG, Siddique R (2015) Recent advances in understanding the role of supplementary cementitious materials in concrete. Cem Concr Res 78:71–80
27. Kannan V, Ganesan K (2014) Chloride and chemical resistance of self compacting concrete containing rice husk ash and metakaolin. Constr Build Mater 51:225–234
28. Kumar AN, Velayutham T (2019) Experimental research on rice husk ash as replacement to cement in construction industry. Int J Recent Technol Eng 8(8):1197–1200
29. Kumar R (2020) Partial replacement of coconut shell ash with cement in concrete. Int J Sci Res 9(8):46–51
30. Kumar R, Malik A, Kashyap VK (2018) Partial replacement of cement with rice husk ash and fine aggregates by coconut shell powder in concrete. Int J Civil Eng Technol 9(4):544–551
31. Kursat E, Ehsan G (2017) Development of eco-efficient self-compacting concrete with waste marble powder using the response surface method. J Clean Prod 144:192–202
32. Lee J, Yang X, Cho SH et al (2017) Pyrolysis process of agricultural waste using CO2 for waste management, energy recovery, and biochar fabrication. Appl Energ 185:214–222
33. Lu Q, Yang XL, Zhu XF (2008) Analysis on chemical and physical properties of bio-oil pyrolyzed from rice husk. J Anal Appl Pyrol 82(2):191–198
34. Madhu P, Livingston TS, Manickam IN (2017) Fixed bed pyrolysis of lemongrass (Cymbopogon flexuosus): Bio-oil production and characterization. Energ. Source Part A: Recovery Util. Environ Eff 39(13):1359–1368.

https://dx.doi.org/10.1080/15567036.2017.1328623
35. Madrid R, Nogueira C, Margarido F (2012) Production and characterisation of amorphous silica from rice husk waste. In WasteEng'2012: Proceedings of the 4th International Conference on Engineering for Waste and Biomass Valorisation
36. Madurwar MV, Mandavgane SA, Ralegaonkar RV (2014) Use of sugarcane bagasse ash as brick material. Curr Sci 107(6):1044–1051
37. Mahesh B, Kumar TM, Nikhil U, Yakaswamy A (2017) Usage of sugarcane bagasse ash in concrete. Int J Eng Res Gen Sci 5(2):218–224
38. Mangi SA, Jamaluddin N, Wan Ibrahim MH, Abdullah AH, Abdul Awal ASM, Sohu S, Ali N (2017) Utilization of sugarcane bagasse ash in concrete as partial replacement of cement. IOP Conf Ser : Mater Sci Eng 271:012001
39. Musthafa S, Basha SM, Bhavani S, Anudeep P, Chakravarhy P, Vali SN (2019) Experimental study on partial replacement of cement by banana leaves ash and glass fiber. International Journal of Research in Advent Technology, Special. 2019:650–655
40. Newman J, Choo BS (2003) Advanced concrete technology 3: processes. Elsevier, England
41. Nur Firdaus MY, Osman H, Metselaar HSC, Rozyanty AR (2016) Preparation and Characterization of Active SiO2 from Cymbopogon citratus Ash Calcined at Different Temperature. Bioresour 11(1):2839–2849
42. Olofintuyi I, Oladapo S (2019) Strength Assessment of Bamboo Trunk Ash (BTA) and Grinded Snail Shell (GSS) As Additives in Self-Compacting Concrete (SCC) Int. Res. J. Innov. Eng. Technol. 3(4):40–43, 2019
43. Olofintuyi IO, Oluborode KD, Adegbite I (2015) Structural value of bamboo leaf ash as a pozzolanic material in a blended portland cement. Int J Eng Sci Res Technol 4(9):171–177
44. Olutoge FA, Oladunmoye OM (2017) Bamboo leaf ash as supplementary cementitious material. Am J Eng Res 6(6):1–8
45. Paulose I, Babu S (2021) Efficiency analysis of banana stem ash as a supplementary cementitious material in concrete. Int Res J Eng Technol 8(6):2956–2962
46. Pawar JR, Khaire AS (2018) Experimental investigation on properties of concrete by partial replacement of cement with banana leaves ash. Int J Res Eng Appl Manag 789–794
47. Prithiviraj C, Saravanan J, Kumar DR, Murali G, Vatin NI, Swaminathan P (2022) Assessment of Strength and Durability Properties of Self-Compacting Concrete Comprising Alccofine. Sustainability. 14:5895. https://doi.org/10.3390/su14105895
48. Rachniyom W, Srisittipokakun N, Kaewkhao J (2019) Comparative study of SiO_2 in biomass ashes at different temperatures. 14(3):12–15
49. Ramezanianpour AM, Hooton RD (2013) Sulfate resistance of Portland-limestone cements in combination with supplementary cementitious materials. Mater Struct 46:1061–1073
50. Rao PP, Kumar AP, Singh BB (2014) A Study on use of rice husk ash in concrete. Int J Educ Appl Res 4(2):75–81
51. Revathi R, Bharathi L, Durgadevi A, Kavipriya D (2018) Experimental study on partial replacement of coarse aggregate by coconut shell and with addition of chicken feather in concrete. Int J Innov Res Manag Eng Technol 3(2):7–13
52. Sahoo N, Kumar A, Samsher (2022) Review on energy conservation and emission reduction approaches for cement industry. Environ Dev 44:100767. https://doi.org/10.1016/j.envdev.2022.100767
53. Siad H, Mesbah HA, Khelafi H, Kamali-Bernard S, Mouli M (2010) Effect of mineral admixture on resistance to sulphuric and hydrochloric acid attacks in selfcompacting concrete. Can J Civ Eng 37:441–449
54. Thomas BS, Yang J, Mo KH, Abdalla JA, Hawileh RA, Ariyachandra E (2021) Biomass ashes from agricultural wastes as supplementary cementitious materials or aggregate replacement in cement/geopolymer concrete: A comprehensive review. J Build Eng 40(7):102332. https://doi.org/10.1016/j.jobe.2021.102332
55. Tijani MA, Olawale SOA, Abdullahi L, Aliyu MA, Ajagbe WO (2020) Effect of sorghum husk ash and calcium chloride on compressive strength of grade 20 concrete. Mater Sci Eng 1036:012054. IOP Conf. Ser.10.1088/1757-899X/1036/1/012054

56. Umoh AA, Ujene AO (2014) Empirical study on effect of bamboo leaf ash in concrete. J Eng Technol 5(2):71–82
57. Wongkhorsub C, Chindaprasert N (2013) A comparison of the use of pyrolysis oils in diesel engine. Energ Power Eng 5(4):350–355
58. Worrell E, Price L, Martin N, Hendriks C, Meida LO (2001) Carbon dioxide emissions from the global cement industry. Annu Rev Energy Environ 26:303–329
59. Zady M (2000) Correlation and simple least squares regression. Clinical laboratory science program. University of Louisville, Louisville, Kentucky
60. Zhou Z, Yang Y, Li X, Li P, Zhang T, Lv X, Liu L, Dong J, Zheng D (2018) Optimized removal of natural organic matter by ultrasound-assisted coagulation of recycling drinking water treatment sludge. Ultrason Sonochem 48:171–180

Figures

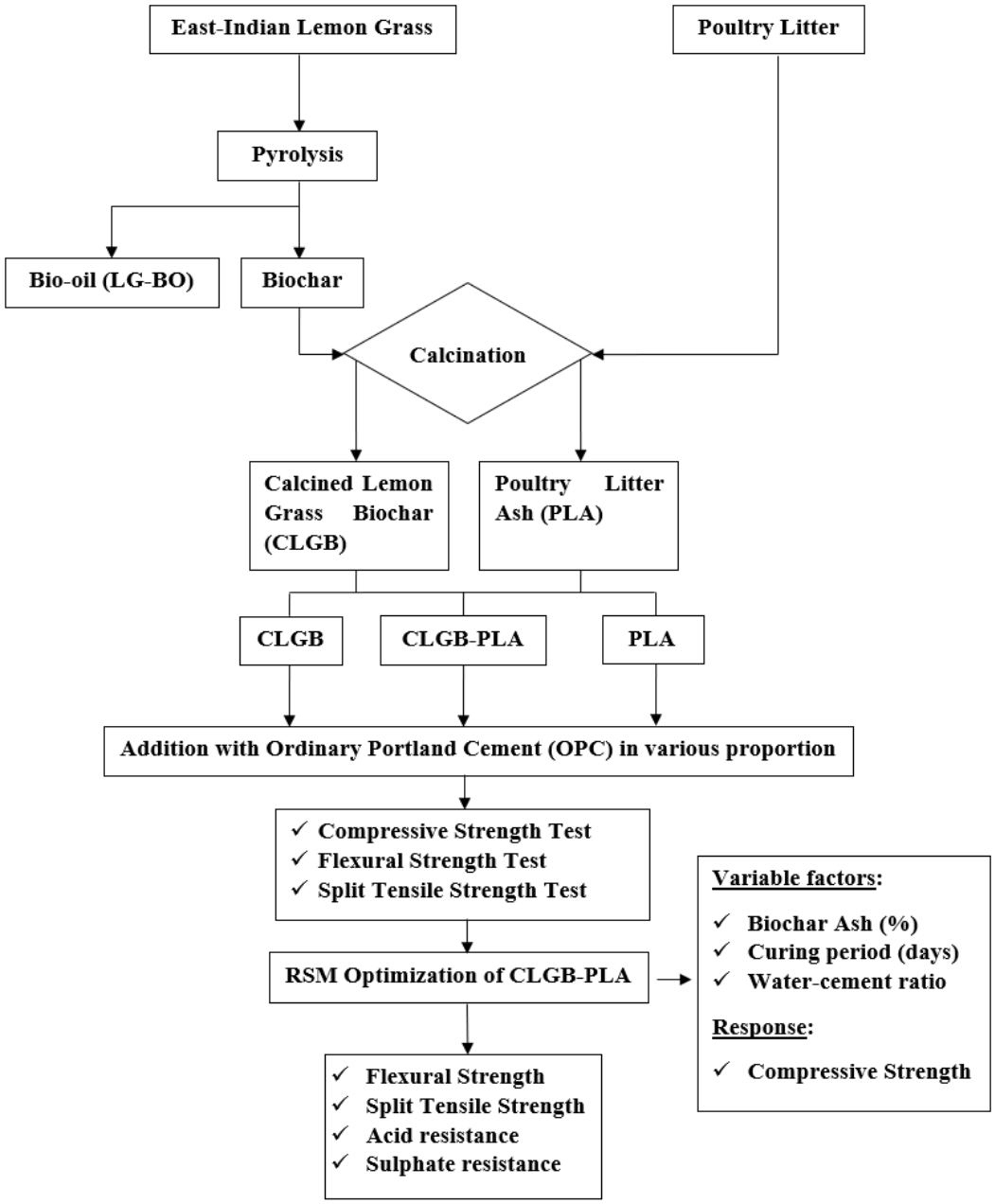

Figure 1

Process flowchart

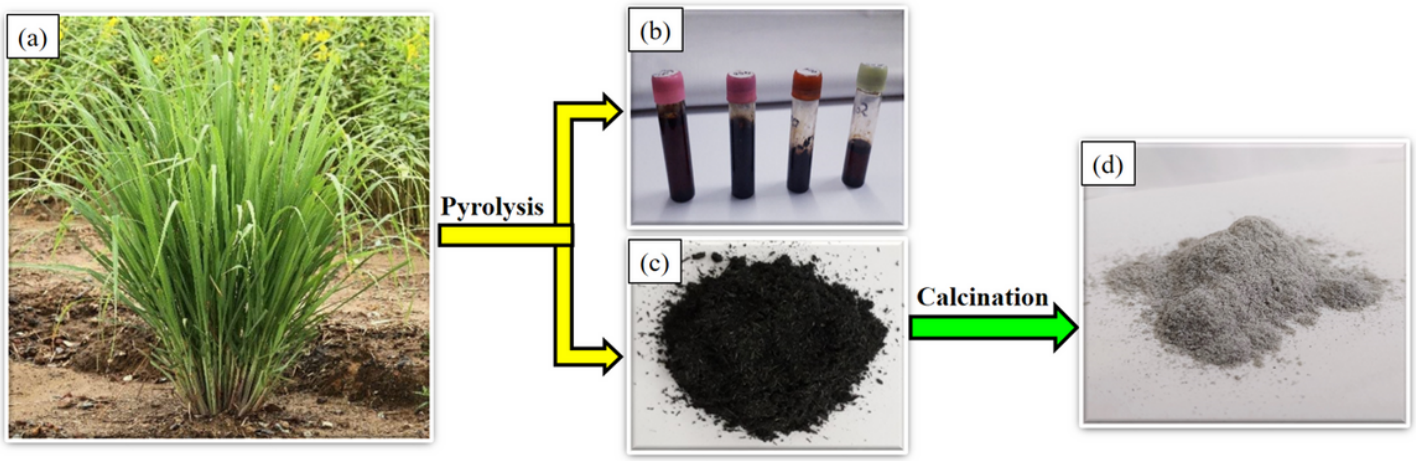

Figure 2

Stages of calcined lemon grass biochar preparation: (a) Lemon grass plant; (b) Bio-oil; (c) Biochar; and (d) Calcined lemon grass biochar

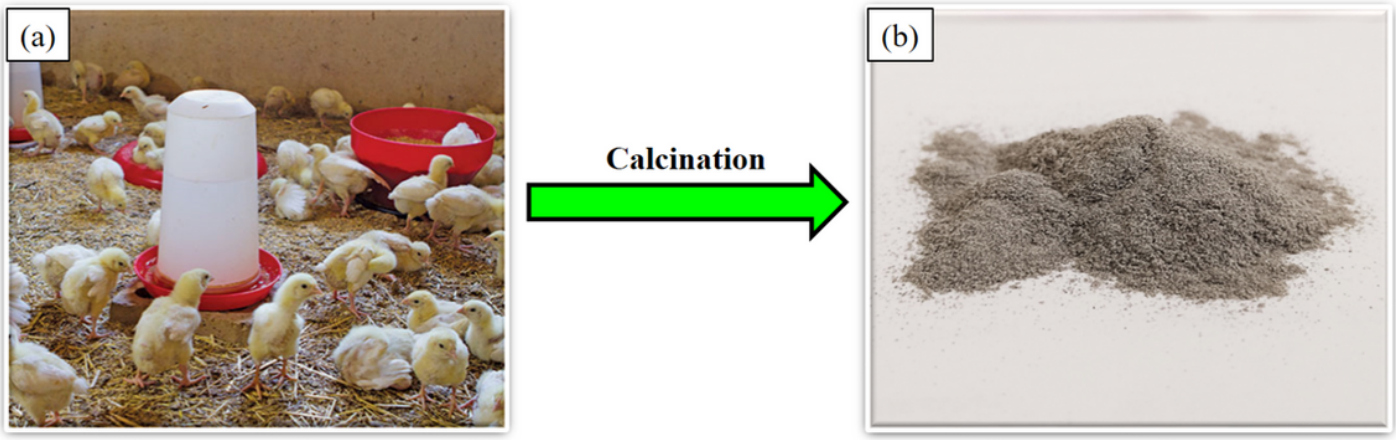

Figure 3

Process of poultry litter ash preparation: (a) Raw poultry litter; (b) Poultry litter ash prepared from dried and grinded sample applying calcination

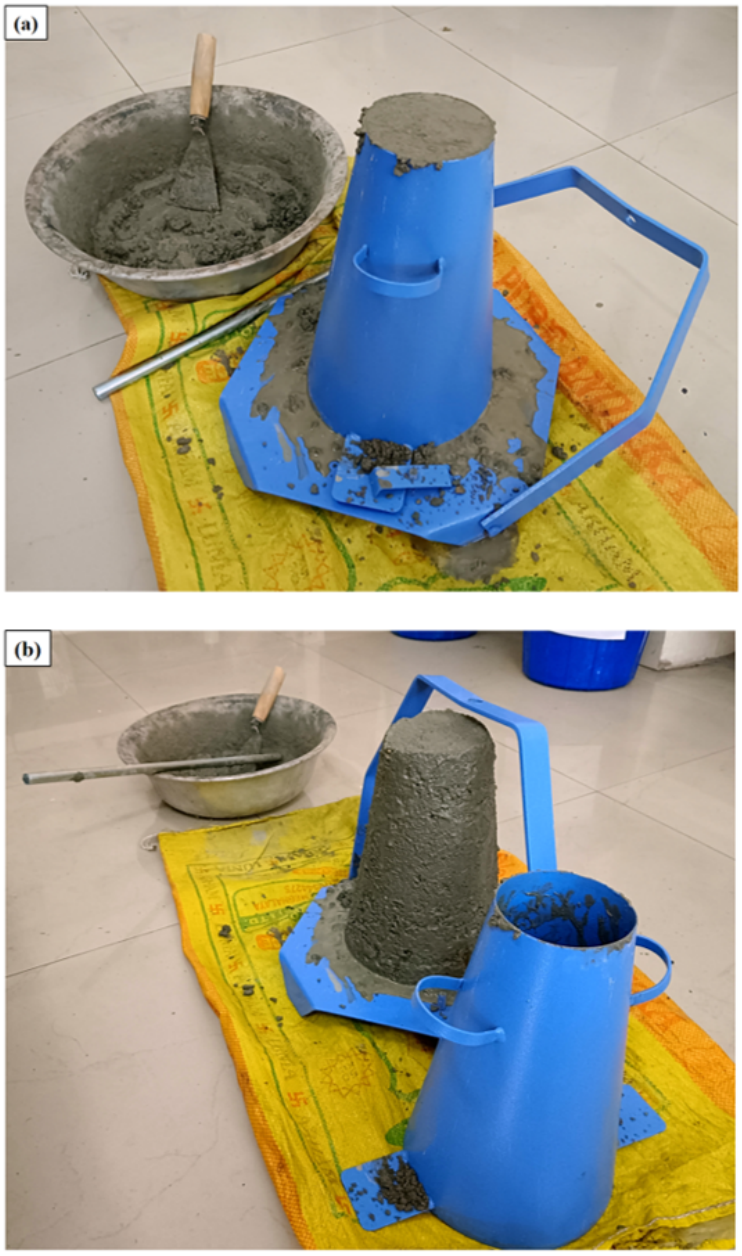

Figure 4

Schematic representation of slump flow analysis (a) Concrete mixture in slump cone apparatus; (b) 25 % PLA mix concrete showing true slump property

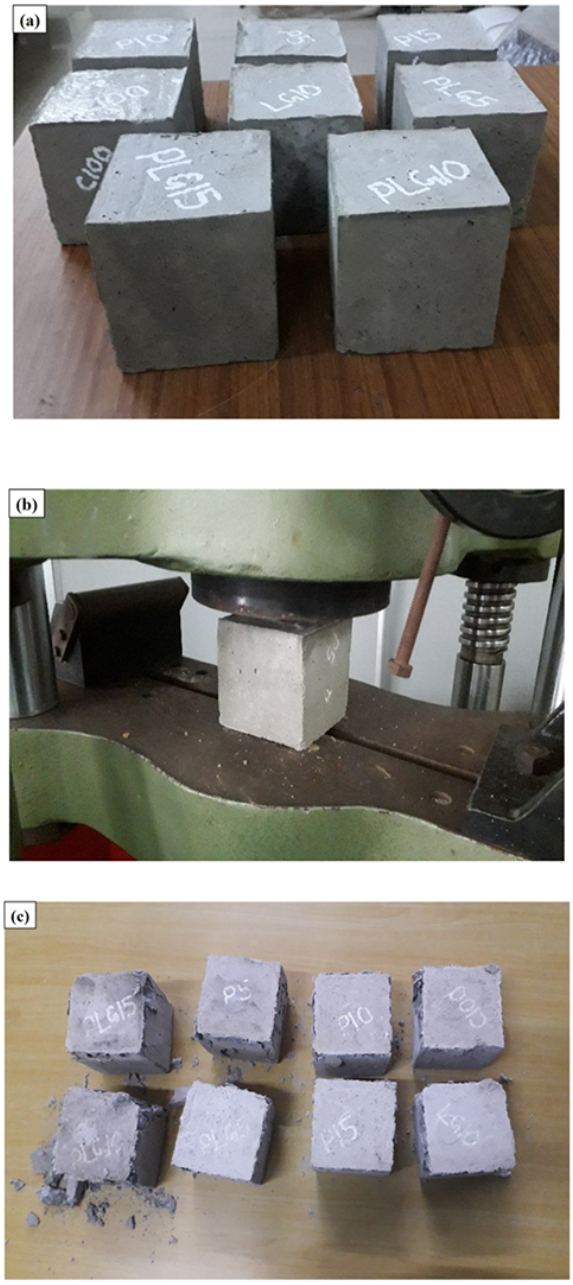

Figure 5

Schematic representation of compressive strength test (a) Prepared cube specimens; (b) Cube placed in universal testing machine; and (c) Cubes after the test

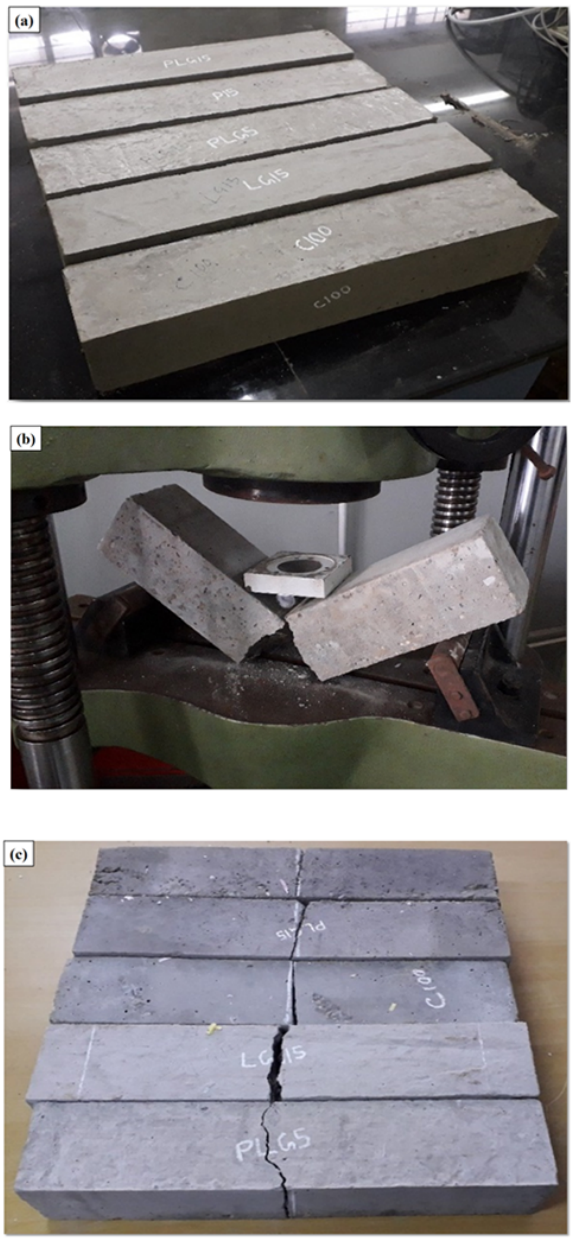

Figure 6

Schematic representation of flexural strength test (a) Prepared beams; (b Beam placed in universal testing machine; and (c) Beams after the test

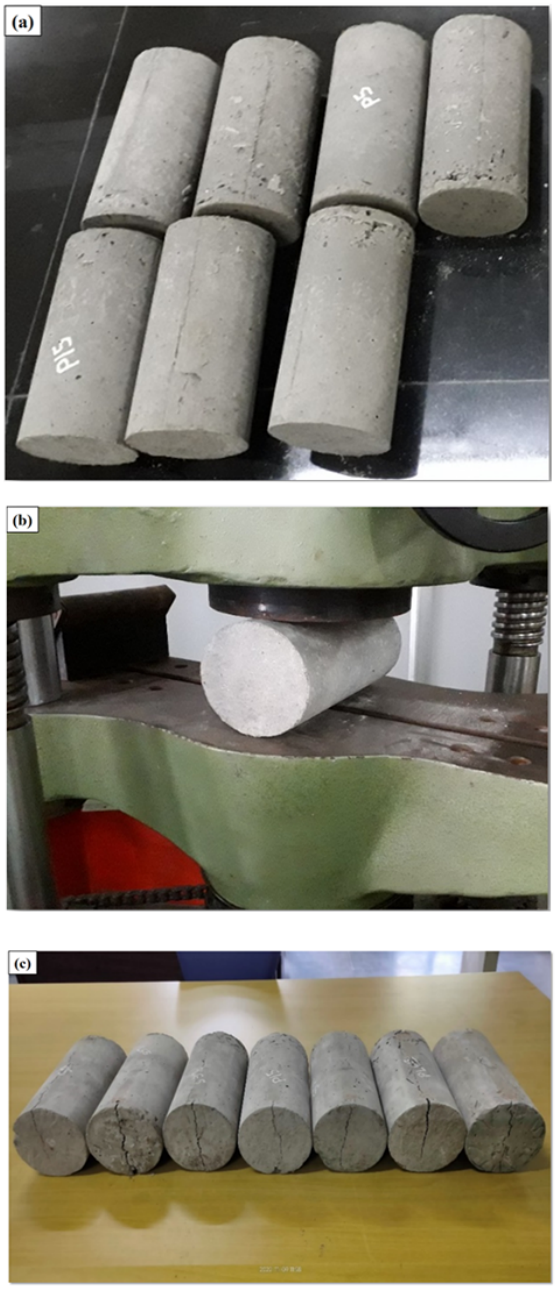

Figure 7

Schematic depiction of split tensile strength test (a) Prepared solid cylinders; (b Cylinder placed in universal testing machine; and (c) Cylinders after the test

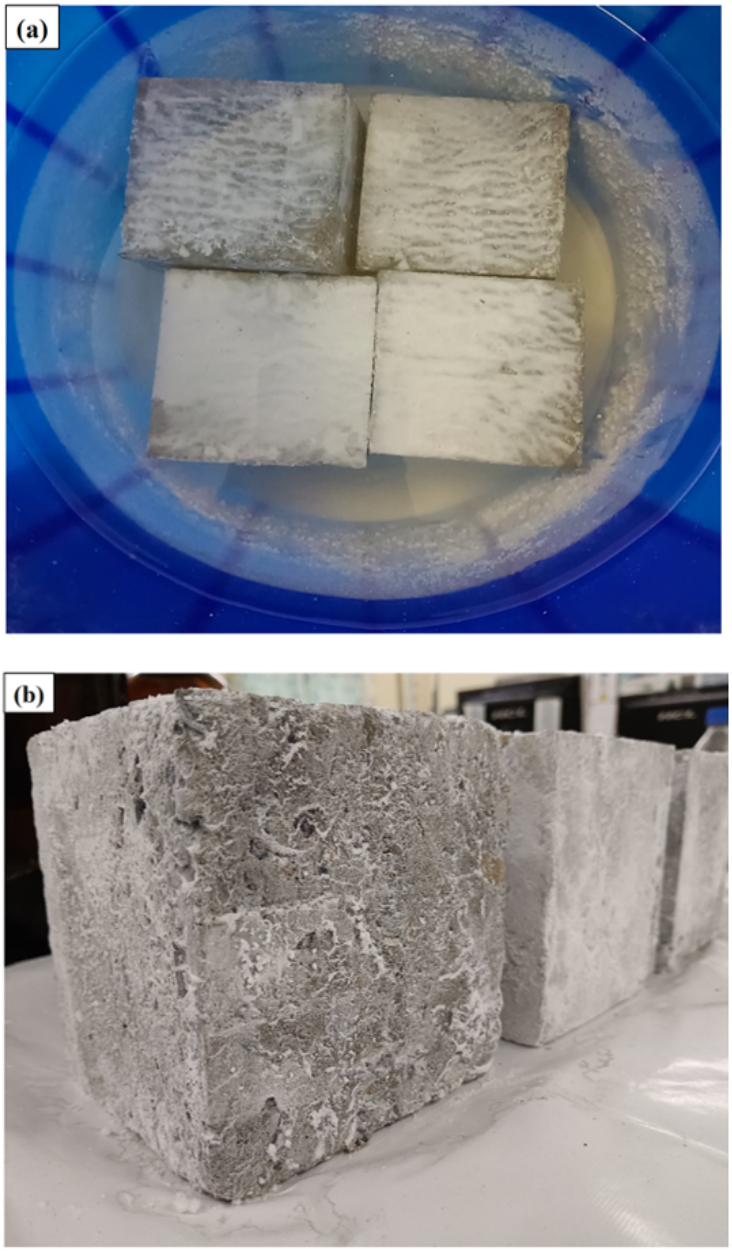

Figure 8

Schematic demonstration of sulphate resistance test (a) Cubes immersed in $MgSO_4$ solution; (b) Cubes after removal from $MgSO_4$ solution

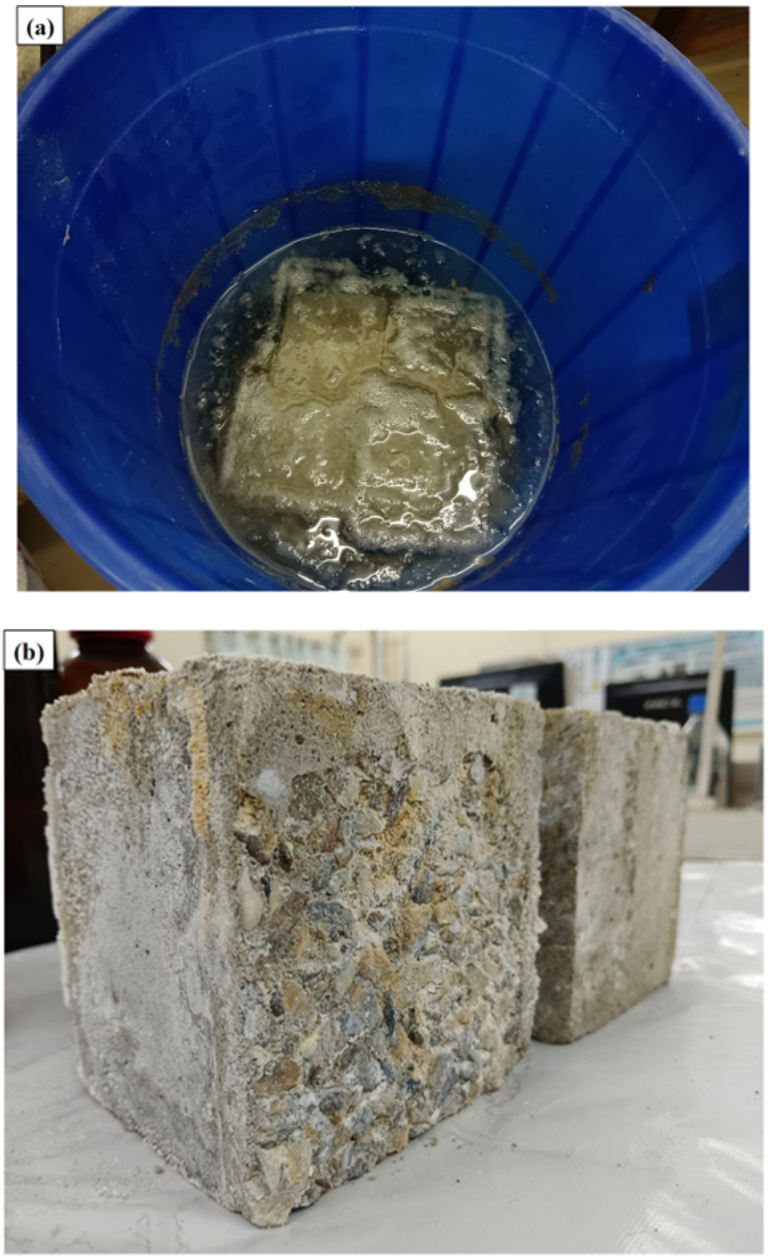

Figure 9

Schematic demonstration of acid resistance test (a) Cubes immersed in acid solutions; (b) Cubes after removal from acid solutions

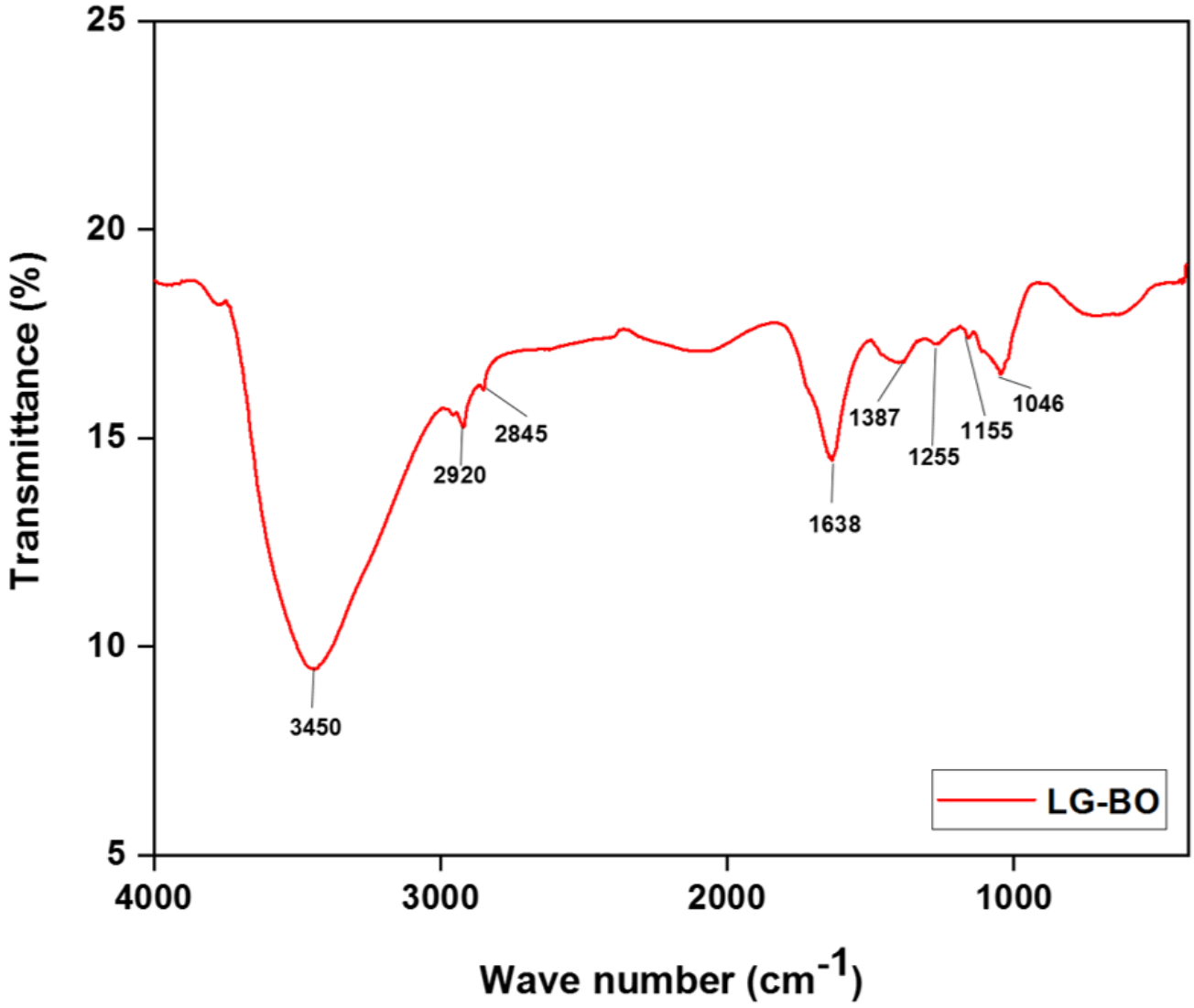

Figure 10

FTIR of LG-BO

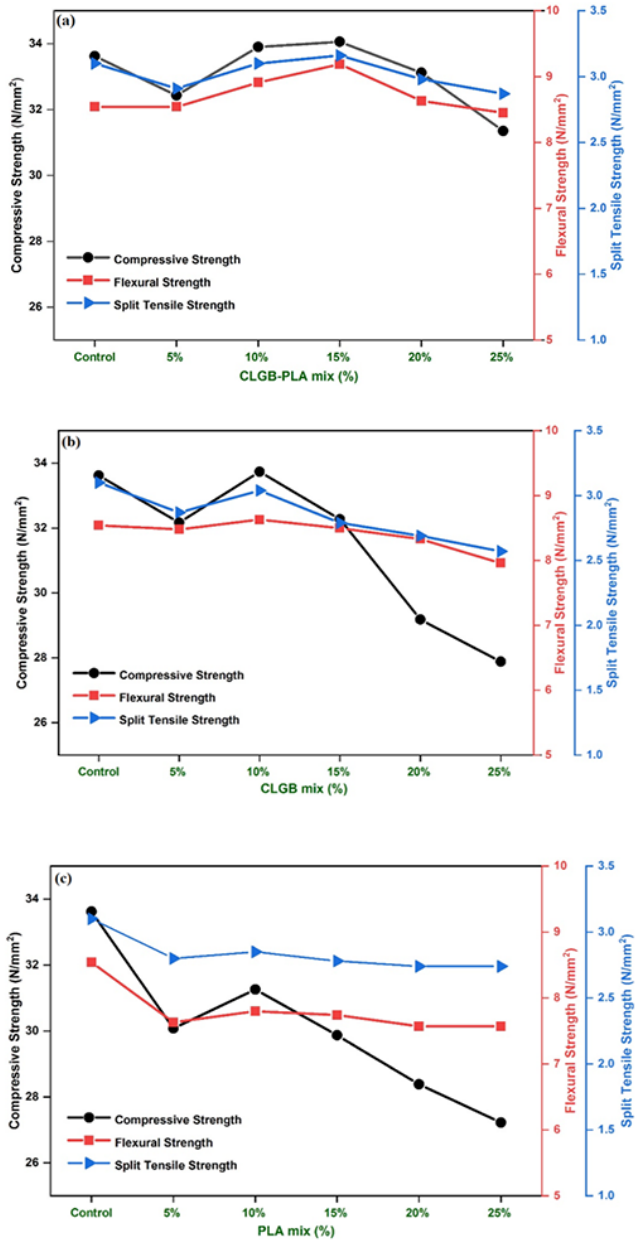

Figure 11

Graphical representation of compressive, flexural and split tensile strength against different percentage of (a) CLGB-PLA mix, (b) CLGB mix, and (c) PLA mix

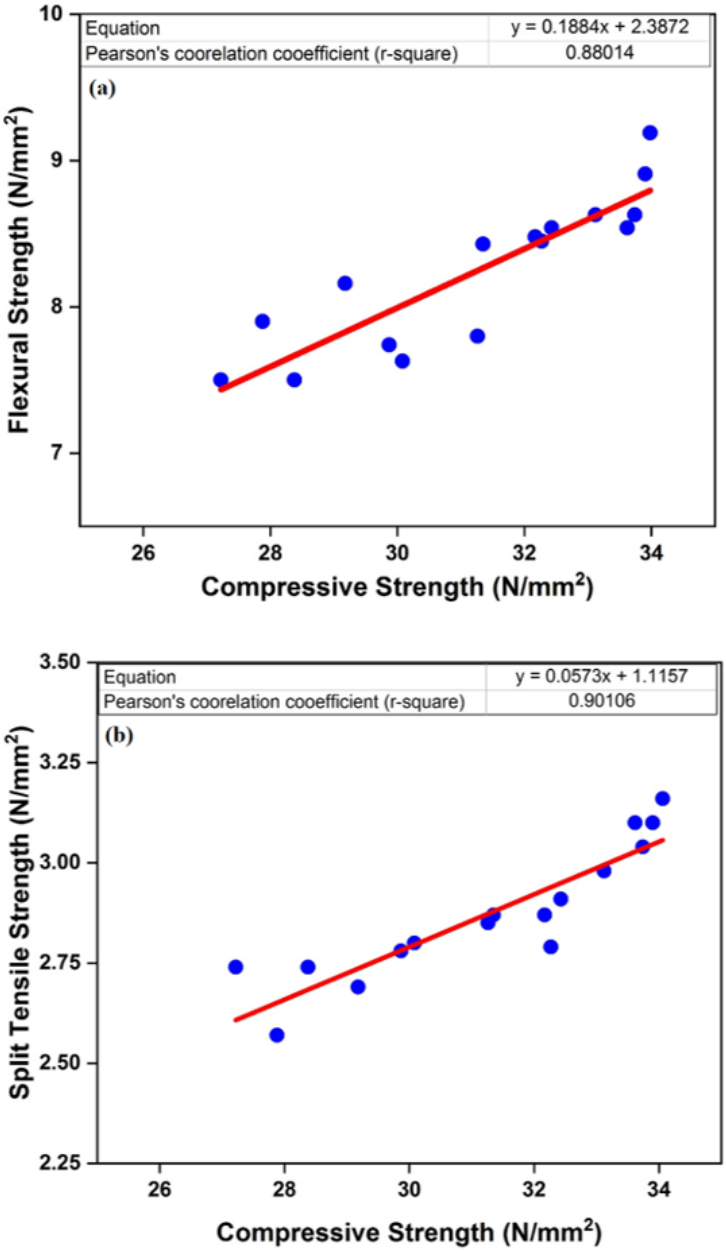

Figure 12

Correlation between (a) compressive and flexural strength (b) compressive and split tensile strength of different specimens

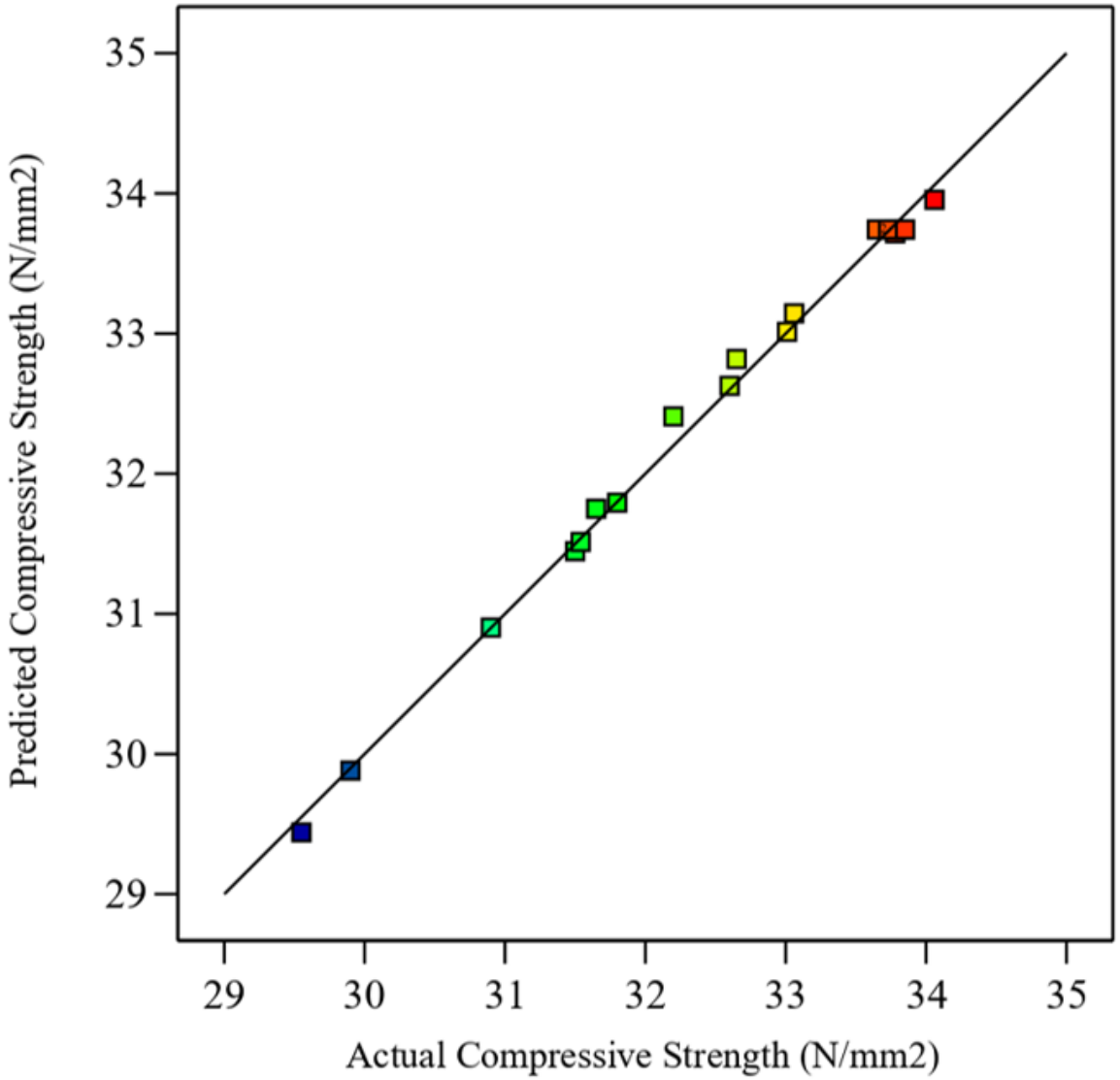

Figure 13

Comparison between actual versus predicted values of compressive strengths

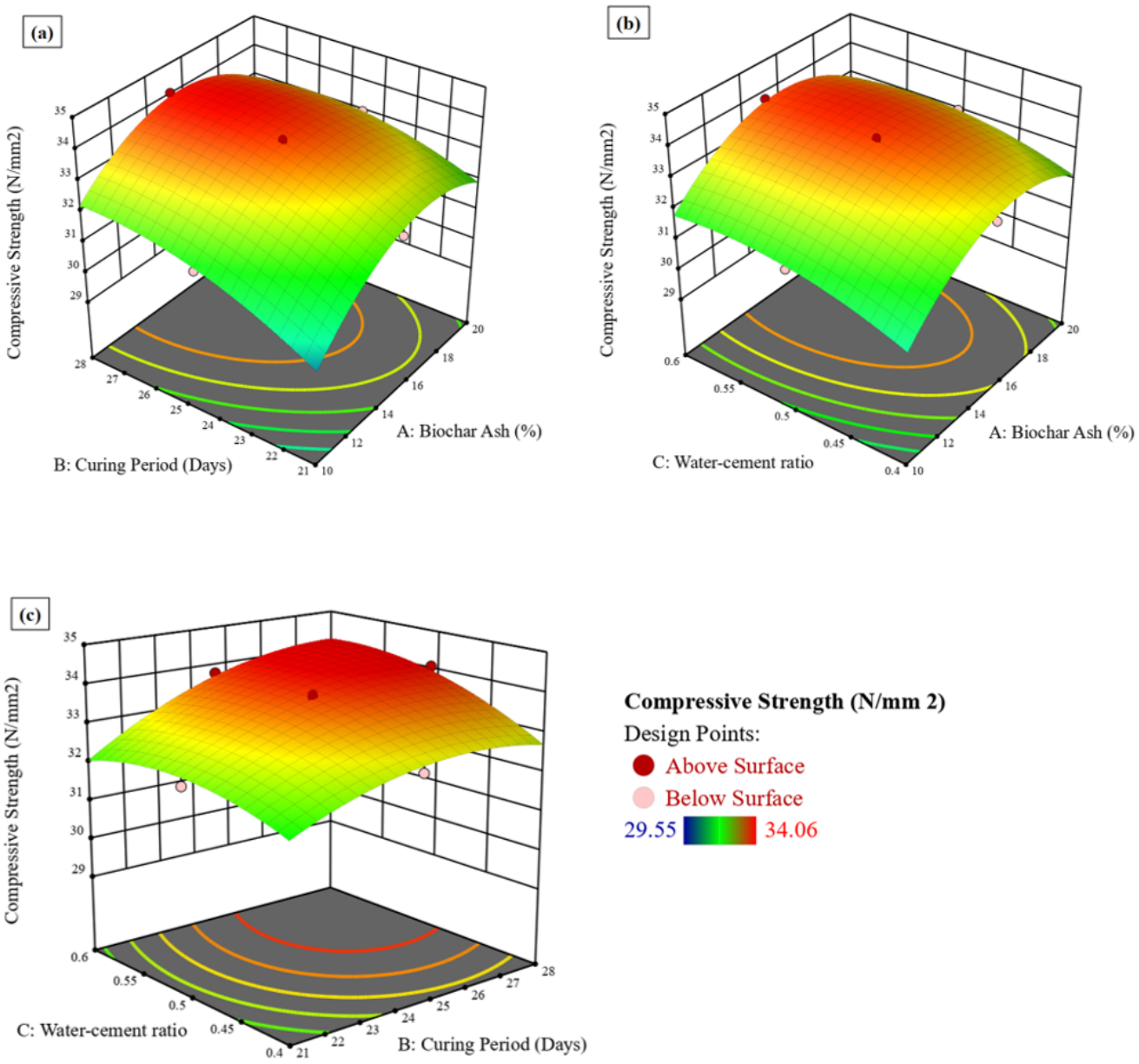

Figure 14

3D response surface illustrating interactive effect of (a) biochar ash and curing period, (b) biochar ash and water-cement ratio, and (c) curing period and water-cement ratio

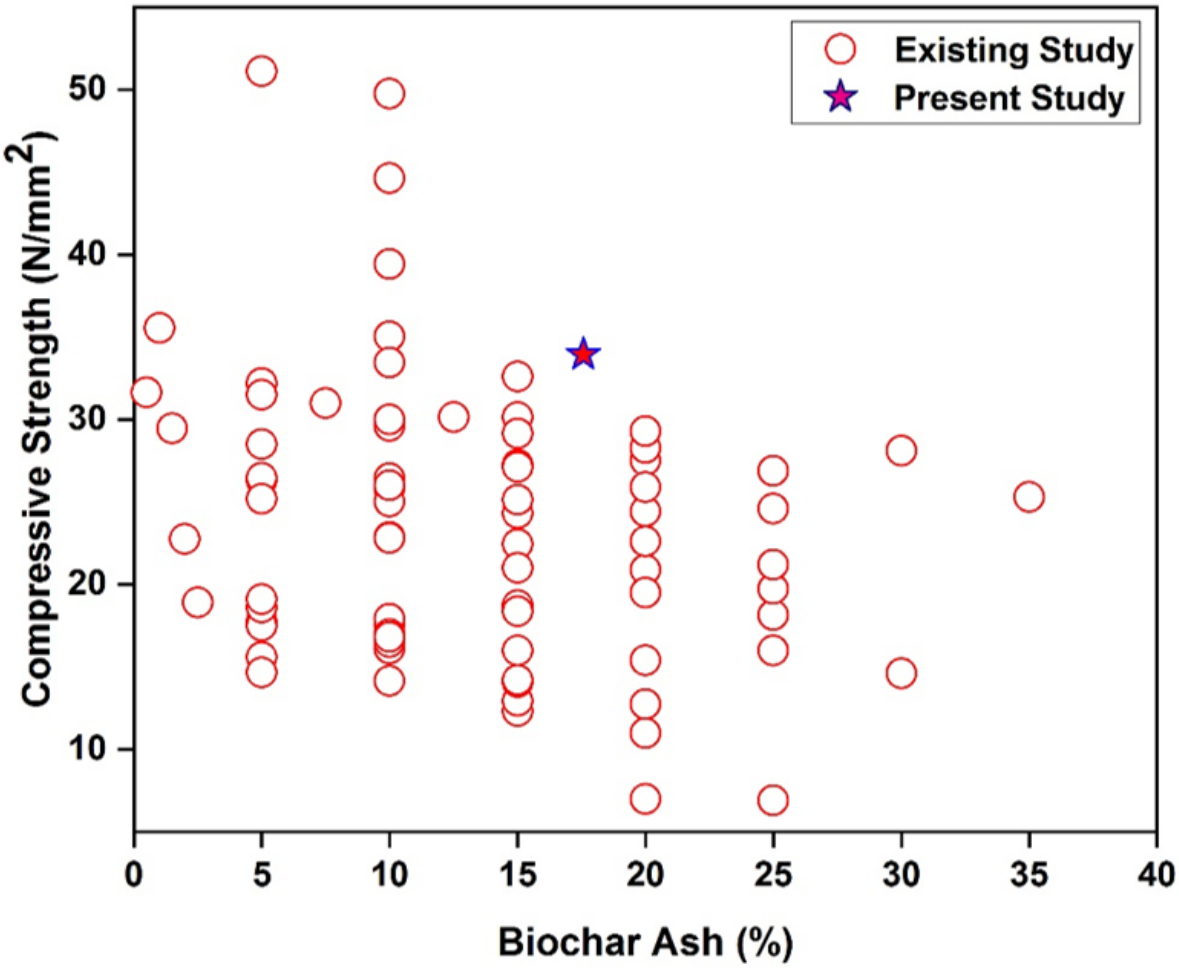

Figure 15

Comparative analysis of compressive strength with existing results

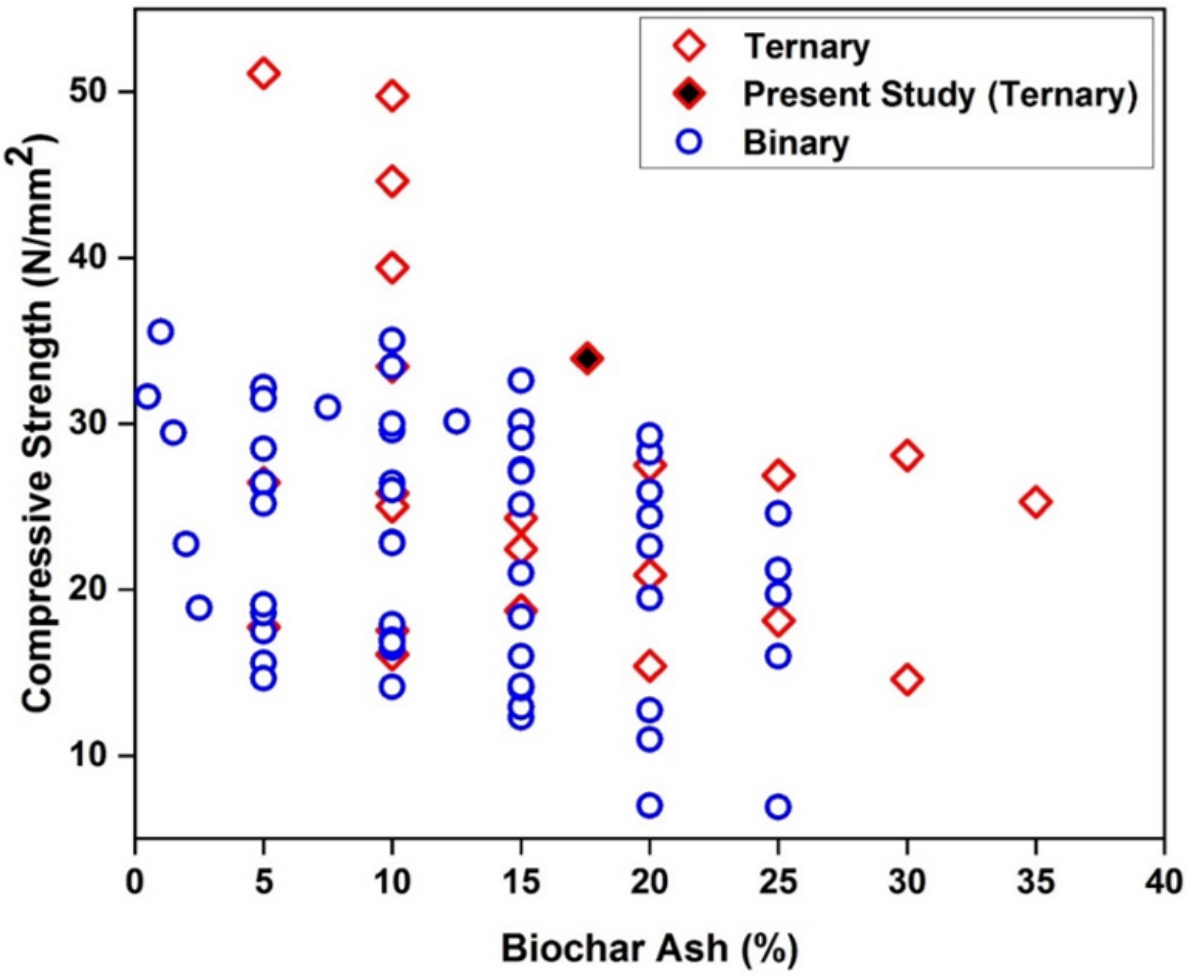

Figure 16

Compressive strength of binary and ternary blended concrete